# TECHNICAL REPORT STANDARD PAGE

1. Title and Subtitle

**Fabrication of Superhydrophobic Surfaces via Air-assisted Electrospray Method**

2. Author(s)

Ling Fei

3. Performing Organization Name and Address

Chemical Engineering
University of Louisiana at Lafayette
Lafayette, LA, 70504

4. Sponsoring Agency Name and Address

Louisiana Department of Transportation and Development
P.O. Box 94245
Baton Rouge, LA 70804-9245

5. Report No.

**FHWA/LA.17/Enter 3-digit Report No.**

6. Report Date

06/29/2022

7. Performing Organization Code

LTRC Project Number: 22-4TIRE
SIO Number: DOTLT1000417

8. Type of Report and Period Covered

Annual
07/01/2021 -06/30/2022

9. No. of Pages

57

10. Supplementary Notes

Conducted in Cooperation with the NASA, NSF

11. Distribution Statement

Unrestricted. This document is available through the National Technical Information Service, Springfield, VA 21161.

12. Key Words

Anti-corrosion, self-cleaning, superhydrophobic surfaces

13. Abstract

In recent decades, superhydrophobic surfaces have received utmost attention due to their novel applications such as self-cleaning, anti-corrosion, anti-fouling, anti-icing coatings, and oil-water separation. The fabrication of such surface coatings requires delicate control over nano- and micro-scale roughness. However, superhydrophobic surface fabrication often involves time-consuming or complicated processes and has little control over surface structures. For instance, the current popular coating fabrication methods include dip coating, blading coating, as well as air gun spray. The first two have no control on surface structures, and the air gun spray tends to be time consuming and have requirement on solvent volatility. To address these problems, an air-assisted electrospray technique is presented in this study to fabricate superhydrophobic coating on glass substrates. The outstanding advantage of this approach is to form a coating with excellent adhesion, high uniformity, and good surface structure controls in a timely manner. This air-controlled electrospray was inspired by the widely applied electrospinning method, thus possessing all the advantages that electrospinning has such as low cost, easy scaling up, and simultaneous solvent evaporation. The air-assisted electrospray nozzle is comprised of two concentric cylindrical needles with the inner needle supplied with solution and outer shell with convective air flow jet from air compressor. The air helps atomize the big solution droplets into small ones so that electrostatic force is able to bring them to target. Similar to electrospinning, solvent can be simultaneously evaporated during the process. This instantly drying spray process eliminates the possibility of cracking due to surface tension from solvent evaporation which is sometimes seen in conventional coating methods, such as dip or blading coating. We used a silicon dioxide nanopowder in the polyacrylonitrile/n,n-dimethylformamide to test out the new method and identified the optimal spray solution ratio of the precursors. In addition, we systematically studied the process parameters involved including concentration, air flow rate, solution infused rate, and power voltage. The optimal conditions of the air-assisted electrospray process for the selected material system were also identified. The static water contact angle of the prepared superhydrophobic surface can achieve 167.1°. The superhydrophobic surface exhibits both remarkable water and oil repellent properties and mechanical robustness against abrasion. Therefore, the presented facile air-assisted electrospray technique can be potentially used for various advanced industrial applications for self-cleaning and anti-corrosion surfaces.

# Project Review Committee

Each research project will have an advisory committee appointed by the LTRC Director. The Project Review Committee is responsible for assisting the LTRC Administrator or Manager in the development of acceptable research problem statements, requests for proposals, review of research proposals, oversight of approved research projects, and implementation of findings.

LTRC appreciates the dedication of the following Project Review Committee Members in guiding this research study to fruition.

***LTRC Administrator/Manager***

[Enter name]

[Enter field of research]Research Manager

***Members***

Enter member's names, one per line

***Directorate Implementation Sponsor***

Christopher P. Knotts, P.E.

DOTD Chief Engineer

# Fabrication of Superhydrophobic Surfaces via Air-assisted Electrospray Method

By
Ling Fei

Chemical Engineering Department
University of Louisiana at Lafayette
Lafayette, LA 70504

LTRC Project No. 22-4TIRE
SIO No. DOTLT1000417

conducted for
Louisiana Department of Transportation and Development
Louisiana Transportation Research Center

The contents of this report reflect the views of the author/principal investigator who is responsible for the facts and the accuracy of the data presented herein.

The contents of do not necessarily reflect the views or policies of the Louisiana Transportation Research Center. This report does not constitute a standard, specification, or regulation.

06/29/2022

# Abstract

In recent decades, superhydrophobic surfaces have received utmost attention due to their novel applications such as self-cleaning, anti-corrosion, anti-fouling, anti-icing coatings, and oil-water separation. The fabrication of such surface coatings requires delicate control over nano- and micro-scale roughness. However, superhydrophobic surface fabrication often involves time-consuming or complicated processes and has little control over surface structures. For instance, the current popular coating fabrication methods include dip coating, blading coating, as well as air gun spray. The first two have no control on surface structures, and the air gun spray tends to be time consuming and have requirement on solvent volatility. To address these problems, an air-assisted electrospray technique is presented in this study to fabricate superhydrophobic coating on glass substrates. The outstanding advantage of this approach is to form a coating with excellent adhesion, high uniformity, and good surface structure controls in a timely manner. This air-controlled electrospray was inspired by the widely applied electrospinning method, thus possessing all the advantages that electrospinning has such as low cost, easy scaling up, and simultaneous solvent evaporation. The air-assisted electrospray nozzle is comprised of two concentric cylindrical needles with the inner needle supplied with solution and outer shell with convective air flow jet from air compressor. The air helps atomize the big solution droplets into small ones so that electrostatic force is able to bring them to target. Similar to electrospinning, solvent can be simultaneously evaporated during the process. This instantly drying spray process eliminates the possibility of cracking due to surface tension from solvent evaporation which is sometimes seen in conventional coating methods, such as dip or blading coating. We used a silicon dioxide nanopowder in the polyacrylonitrile/n,n-dimethylformamide to test out the new method and identified the optimal spray solution ratio of the precursors. In addition, we systematically studied the process parameters involved including concentration, air flow rate, solution infused rate, and power voltage. The optimal conditions of the air-assisted electrospray process for the selected material system were also identified. The static water contact angle of the prepared superhydrophobic surface can achieve 167.1°. The superhydrophobic surface exhibits both remarkable water and oil repellent properties and mechanical robustness against abrasion. Therefore, the presented facile air-assisted electrospray technique can be potentially used for various advanced industrial applications for self-cleaning and anti-corrosion surfaces.

# Acknowledgments

This research is funded by the Louisiana Transportation Research Center under No. DOTLT1000417. Also, we would like to thank all the graduate and undergraduate students' assistance in experimental set up and experimentation.

# Implementation Statement

The simple and straightforward air-assisted electrospray method represents an import technique addition to the current field of self-cleaning coating for various potential engineering and daily use applications.

# Table of Contents

# List of Tables

# List of Figures

# Introduction

In recent decades, self-cleaning materials have attracted growing attention in both academic research and industrial development, due largely to the inspiration by many biological surfaces in nature, such as lotus leaves, rose petals, butterfly wings, desert beetles. Achieving a superhydrophobic surface thus has received utmost attention to accommodate such development. These superhydrophobic surfaces exhibit a combination of micro/nano hierarchical roughness and low surface energy, which result in the special water repellency behavior.[1-4] Superhydrophobic surfaces have contact angles exceeding 150$^{o}$ in water basis.[5] The water droplets can easily roll off of the superhydrophobic surface due to its low contact energy between solid and liquid. Therefore, these surfaces obtain a variety of novel functionalities consisting of anti-fouling, oil-water separation, anti-icing, anti-bacteria, self-cleaning, anti-graffiti, and various other areas.[6-11]

Researchers have proposed various approaches to fabricate superhydrophobic coatings, including dip coating,[12] electrospinning,[13] thermal oxidation,[14] chemical vapor deposition,[15] spraying,[16,17] plasma and chemical etching,[18] sol-gel,[19,20] lithography,[21] and spin coating.[15] Conventional air gun spraying is one of the popular approaches to deposit the superhydrophobic coating on a variety substrates. Recently, Zhu et al. demonstrated a method of spraying carbon nanotubes and silicon dioxide suspension onto glass slides.[20] After thermal treatment and surface fluorination, a transparent superamphiphobic coating was formed. Superamphiphobic surfaces exhibit static contact angles greater than 150$^{o}$ for both polar and nonpolar liquids.[22] This approach of spraying onto a small glass slide (approximately 8 x 2.5 cm) required a large amount of chemical solvent. For instance, 0.1g of carbon nanotubes was dispersed in 130mL mixture of tetraethyl orthosilicate and ethanol (volume ratio 1:25). Namely, the spray precursor solutions are very dilute and only volatile solvent can be used, due to the requirement of solvent evaporation in the coating process. Similarly, Chen et al. fabricated superhydrophobic coating on both hard and soft substrates via conventional spraying method.[23] The coating was achieved by repeated spraying of adhesive followed by silicon dioxide for up to 10 cycles. Many of these conventional spraying approaches successfully produce superhydrophobic surfaces with an excellent self-cleaning performance and sufficient mechanical robustness against harsh environmental conditions. However, those procedures involved a large amount of volatile solvent or a time-consuming process.

To address these challenging problems while maintaining self-cleaning capacity, a simple air-assisted electrospray technique is used in this study to fabricate superhydrophobic coating with good process control and coating properties. Air-assisted electrospray technique has a flexibility in the precursor concentration or solvent volatility. This technique was inspired by the widely applied electrospinning method, thus possessing all the advantages that electrospinning has such as low cost, easy scaling up, and simultaneous solvent evaporation. It has been used in different types of electrode preparation, such as battery, supercapacitor, fuel cell, and solar cell.[24, 25] Recently, the air-assisted electrospray approach has been used successfully to achieve superhydrophobic surfaces. Heo et al. prepared a superhydrophobic polytetrafluoroethylene nanoparticle surface with excellent scale-up application in the bag filter industry via the air-assisted electrospray method.[26] Niknejad et al. recently reported the fabrication of dual-layer nanofibrous polyacrylonitrile (PAN)/ styrene-acrylonitrile (SAN) membrane and polystyrene microbeads-reinforced membranes using the air-assisted electrospraying process, thereby significantly reducing the pore wetting and permeation problems of the membrane distillation process.[27] The unique advantage of this approach is to form a coating layer with excellent adhesion and high uniformity in a timely manner.[28] The solvent quickly evaporates resulting in a dry coating layer instantly during the spraying process.[24] Hence, this instantly drying spray process eliminates the possibility of cracking due to surface tension from solvent evaporation which is sometimes seen in conventional coating methods, such as dip coating or blading. The air-assisted electrospray technique is relatively straightforward and easy to scale up. In view of this, an effort to broaden the application prospect of superhydrophobicity on transparent surfaces via the air-assisted electrospray method was targeted in this paper with cost-effective materials and advanced self-cleaning capacity.

In this work, a mixture of silicon dioxide nanopowders and polyacrylonitrile/n,n-dimethylformamide solution was used to test the new method and assess its potential for surface coating applications. The process parameters involved including concentration, air flow rate, solution infused rate, and power voltage were thoroughly investigated. Further, different methods such as blading and dip coating were demonstrated for the better comparison of the quality and water repellent behavior of coatings. The wettability behavior of the surfaces was analyzed with contact angle measurement and correlated with the surface structures. A series of tests consisting of sandpaper abrasion were conducted to examine the reliability of the coating against harsh environmental conditions. The results of this study could lead to the potential use in various industrial applications of self-cleaning and anti-corrosion surfaces.

# Literature Review on Superhydrophobic and Transparent Surfaces

## 1. Introduction

Many biological surfaces in nature exhibit self-cleaning capabilities.[29] Among them, lotus leaves are the most well-known examples. Water droplets spill on the leaf, not wetting the surface, rolling off easily. As the water moves across the surface, dirt particles are washed away, allowing the lotus' leaves to stay clean always even though they grow in mud. This phenomenon is referred as the "lotus effect".[30] Other similar surfaces can be found in butterfly wings, rose petal, rice leaf, and insects' shell as shown in Figure 1a. These surfaces usually have a water contact angle (WCA) larger than 150° and a small sliding angle (SA) (usually less than 5°). Namely, this type of behavior is indicative of a superhydrophobic surface.

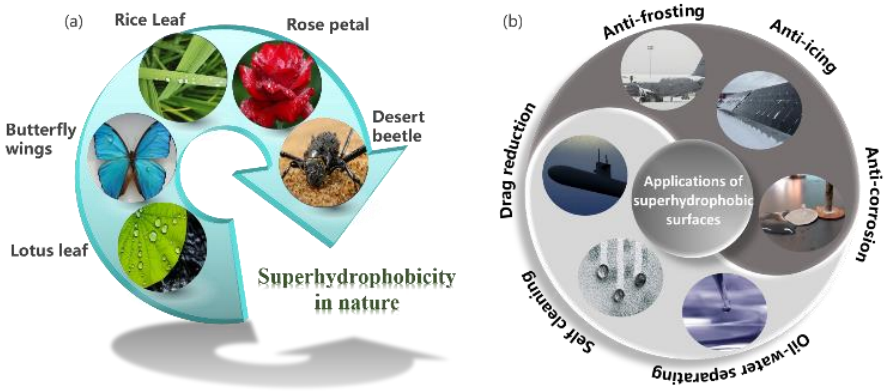


**Figure 1.** (a) Examples of superhydrophobic surfaces in nature; (b) the properties and corresponding applications of superhydrophobic surfaces

Inspired by the lotus effect in nature, many artificial self-cleaning surfaces which mimic the properties of these natural surfaces, have been designed and produced for various applications. For example, paints and textiles with superhydrophobic properties can decrease, even eliminate, the requirement of chemical detergents and high labor costs of cleaning. In addition to self- cleaning functionality, its excellent water repellency can promote anti-icing, antifogging, anti-fouling, anti-scaling, anti-corrosion properties, and drag reduction (Figure 1b), further expanding the range of important applications.[31] Some exemplary applications include ultra-high efficiency windmills, high-speed boats, ice-resistant surfaces in airplanes, microfluidic systems, and membranes for selective separation (e.g. oil-water, gas and liquid).[32] It is also worth mentioning that almost all

natural superhydrophobic surfaces and most synthetic ones are not transparent, severely limiting the application in optics industry. To enable the applications of superhydrophobic surfaces to optical and electronic devices such as solar cell panels, automobile glass, safety goggles, smart windows, greenhouse, camera lenses, and electronic screens, it is equally critical to maintain high optical transparency.[33] Such transparent and self-cleaning surfaces represent one of the key advancement directions in the future optical/electronic devices.

However, it has been very challenging to obtain a transparent superhydrophobic medium while maintaining high optical quality and mechanical durability, mainly because the surface features required for superhydrophobicity often leads to severe light scattering, resulting in nearly opaque or translucent surfaces.[34] In this review, the fundamentals and conditions that govern superhydrophobicity and optical transparency will be discussed. Selected examples of design and fabrication of superhydrophobic and transparent surfaces will be presented. Future perspectives will be offered. This main goal of this review is to help readers gain a quick understanding of the proposed topic, self-cleaning and transparent surfaces, and inspire new research in this area.

## 2. Superhydrophobicity

### 2.1. Wetting behavior of superhydrophobic surface

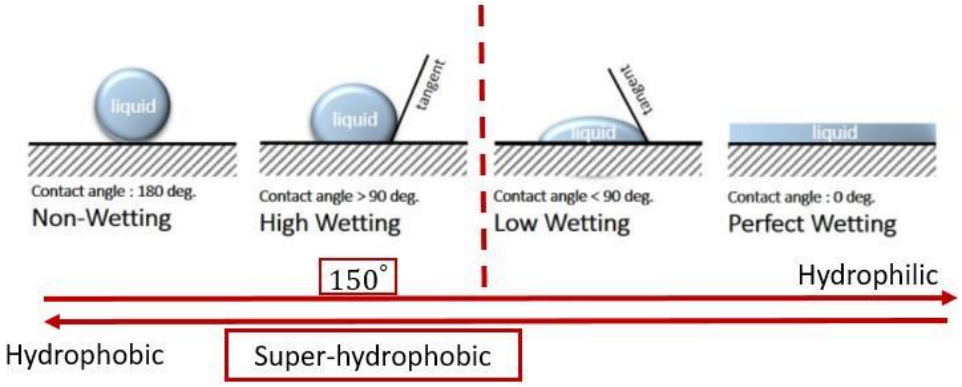


**Figure 2.** Different wetting properties in relationship with contact angle.[36]

Wettability refers to the ability of a liquid to maintain contact with a solid surface as a result of intermolecular interactions. When a liquid drop is in contact with a surface, it can form a sphere or wet the surface completely, representing the anti-wetting and super wetting behavior, respectively.[32a] Several parameters including contact angle, contact angle hysteresis, sliding angle, and shedding angle can be measured to evaluate the wettability. Among them, contact angle (CA), formed at the three-phase boundary where solid, liquid,

and vapor meet, is the most decisive factor of wettability.[35] The contact angle is an indicator of the molecular interaction strength of the three phases. At any given temperature and pressure, a given system of solid, liquid, and vapor has its unique equilibrium contact angle. On the basis of water contact angle, wetting behavior can be classified into four different regimes: $0° < \theta < 10°$, $10° < \theta < 90°$, $90° < \theta < 150°$, and $150° < \theta < 180°$, corresponding to the terms of superhydrophilic, hydrophilic, hydrophobic, and superhydrophobic, respectively. When the liquid is distributed on the surface, a small contact angle represents better wetting; while large contact angle is formed when there is lower contact area between solid and liquid, representing bad wetting. A schematic illustration that summarizes the relationship between contact angle and wetting behavior is demonstrated in Figure 2.[36] Accordingly, the superhydrophobic surfaces in this context has unfavorable water wetting behavior.

CA measurement is a very convenient way to evaluate the surface wettability; however, CA measurement can be influenced by several factors including: the size and weight of the liquid drop, the height of the liquid dropping on the substrate; and the determination of baseline at the contacting surface.[37] Therefore, implementation of standard operating procedures and universal guidelines are important for non-biased measurements and results.

## 2.2. Fundamentals of superhydrophobic surfaces

### 2.2.1. Surface roughness and energy

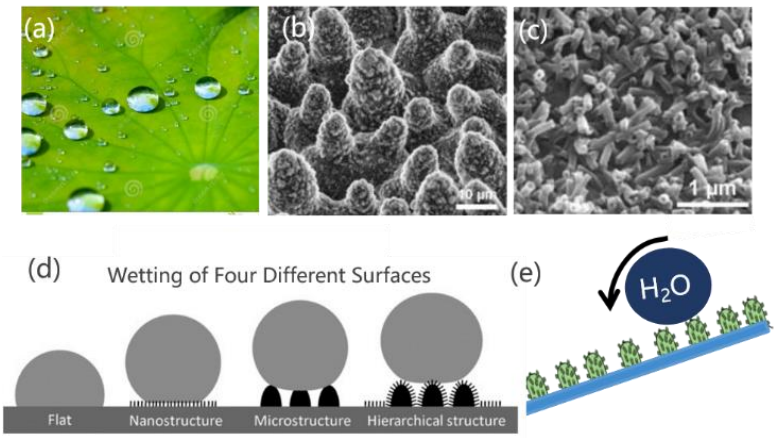


**Figure 3.** Surface roughness and energy. (a) non-wetting water droplets on lotus leaf at macroscale; (b) microscale epidermal cells on the leaf; (c)the nanoscale epicuticular wax tubes on the epidermeral cells;[38] (d) wetting behavior on the surfaces with different structures;[39] (e) schematic illustration of water droplet sliding off the hierarchical structures of lotus leaf.

The two key properties that govern the wettability of surfaces are surface roughness and surface chemistry. In general, the rougher the surface is, the larger the contact angle creates. In addition, surfaces usually carry a specific energy, also referred as surface tension, due to the fact that atoms or molecules of liquid and solid have less chemical bonding at the surface. The chemical structure of the materials defines the surface tension, which in return, partially determines the wettability and adhesion of the materials.

Surface tension/energy can be either measured in energy per unit area ($J/m^2$) or force per unit length (N/m). Low surface energy results in hydrophobic properties while high surface energy leads to hydrophilic properties. Plastics typically have low surface energy, whereas metals tend to have high surface energy. The combination of high surface roughness and low surface energy leads to superhydrophobic surfaces. Surface structures/roughness can trap a good amount of air to increase the water contact angle due to the reduced solid-liquid contact area. While surfaces with low surface energy have dramatically reduced opportunities to bond with water molecules. Take lotus leaf as an example, it has a water contact angle as large as 161.0 ± 2.7° and a sliding angle as small as approximately 2°, exhibiting superhydrophobic properties.[30] As shown in Figure 3a-c, the lotus leaf surface is very rough at the micro and nanoscale.[38] In detail, it has a papillae structure formed with numerous epidermal plant cells at microscale, and at nanoscale with epicuticular wax tubes grown on the surface of the papillae. The roughness is essential to retain air trapping when contacting with water. As shown in Figure 3d, the maximum wettability angle is obtained for water on a flat surface, and the minimum on the roughest surface.[39] Also, Gao et al. studied why two length scales of topography are important for the lotus effect and found the two important reasons involving the kinetics of droplet movement and the thermodynamics of wetting.[40] In addition to roughness, the epicuticular wax has low surface free energy. As a result of both, lotus leaves exhibit superhyphobicity allowing water to roll off easily (Figure 3e). Inspired by natural surfaces, designing hierarchical structures for roughness and modifying surface chemistry for low energy are critical to construct artificial superhydrophobic surfaces.

### 2.2.2. Wetting model

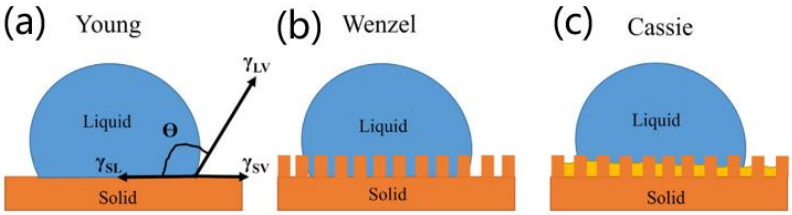


**Figure 4**. Different wetting models.[32a]

Developing a thorough understanding of superhydrophobicity requires a fundamental knowledge of the relationship among surface energy, roughness, and wettability. Several wetting models have been proposed to calculate contact angle on the surface including Young's model, Wenzel's model, and Cassie-Baxter's model as shown in Figure 4.[32a] Young's model, developed by Young in 1805, was the earliest model.[41] In this model, surface roughness is ignored describing the scenario of a drop of liquid on an ideal flat surface. Young indicated that three interfaces exist: solid-liquid (SL), liquid-vapor (LV), and solid-vapor (SV). Correspondingly, the three surface tensions are presented. As shown in Figure 4a, using γ to represent the surface tension and Θ for Young's contact angle, the equilibrium contact angle on the smooth solid surface, the following equation must be held true for the force to balance at x direction:

$$\sum F = \gamma_{SV} - \gamma_{SL} - \gamma_{LV} \cos\theta = 0$$

Rearranging the equation, the Young's equation is expressed as:

$$\gamma_{SV} = \gamma_{SL} + \gamma_{LV} \cos\theta$$

If further transformed and solved for $\cos\theta$, the equitation becomes:

$$\cos\theta = \frac{\gamma_{SV} - \gamma_{SL}}{\gamma_{LV}}$$

From this equation, it is evident that the contact angle is decided by the surface energies of each interface. The value of contact angle is therefore a result of the thermodynamic equilibrium of the free energy at the solid-liquid-gas interface.[32a]

If $\theta$ = 0, liquid spreading occurs, a liquid thin film will form; $\theta$ <90°C, wetting is favorable; $\theta$ > 90°C, wetting is not favorable. Note that the critical surface energy is the surface energy at which complete wetting occurs.

In reality, most surfaces are not smooth. As a result, roughness and other surface conditions profoundly affect the wetting properties, rendering Young's model to be inappropriate for evaluation. Therefore, Wenzel's model was introduced in 1936.[33a, 42] In Wenzel's model (Figure 4b), the assumption is that the liquid droplets is in complete contact with the surface and can pass into the grooves of the rough surface. Additionally, the surface is assumed to have chemical homogeneity. The mathematical form of Wenzel equation is shown below:

$$\cos\theta^w = r\cos\theta$$

Where $\theta^w$ represents the Wenzel contact angle, $\theta$ is Young's contact angle, the equilibrium angle on an ideal surface of the same materials, and r, the surface roughness factor which is defined as the ratio of real surface area to apparent surface area. For idea

flat surfaces, r=1. Since all real surfaces are not smooth at molecular level, r is considered to be greater than 1.
At the condition of r > 1, $\cos\theta^w > cos\theta$
With this relationship holds true, two situations will occur:
(1) if $\theta$ < 90°, then $\theta^w < \theta$
(2) if $\theta$ > 90°, then $\theta^w > \theta$.
Physically, it means roughness will make a hydrophilic surface more hydrophilic and a hydrophobic surface even more hydrophobic.

As mentioned, Wenzel's model assumes homogeneous wetting, namely, the liquid is considered to wet through all surface cavities, leaving no dry area. Real surfaces are very often neither perfectly flat nor homogeneous. Additionally, surfaces with extra high roughness or porous structures (very large r), the absolute value of the right side in Wenzel equation may be greater than 1, where Wenzel model is clearly inadequate and flawed. Herein, the Cassie–Baxter model was proposed for rough and heterogeneous surfaces in 1944.[43] When the surface becomes rougher, it is difficult for liquid to pass into the grooves due to the air packets trapped inside, thus liquid is only in contact with the solid at the roughness tips. The surface with air trapped in cannot be wetted by the liquid as shown schematically in Figure 4c.[32a] The apparent contact angle is closely related to the fraction of the surface that is in contact with liquid. The mathematical equation for the Cassie–Baxter model is: $\cos\theta_{CB} = f_1 cos\theta_1 + f_2 cos\theta_2$ and $1 = f_1 + f_2$
$f_1$ and $f_2$ are the ratio of the liquid-solid interfacial area and the ratio of the liquid-air packets interfacial areal among grooves. $\theta_1$ and $\theta_2$ are contact angle of liquid with solid and air, respectively. Since air is trapped in the grooves, this part of surface can be considered to be in non-wetting status. In other words, $\theta_2$ is 180°. Therefore, bringing in the value of $\theta_2 = 180°$ and combining the two equations above result in the following expression: $\cos\theta_{CB} = f_1(cos\theta_1 + 1) - 1$
Water drops on lotus leaves have many air packets existing underneath, fitting the Cassie–Baxter model very well. In addition to the three above mentioned models, many improved models have also been developed for specific cases of wetting.[32a, 44]

### 3. Superhydrophobicity and transparency

Transparency is a physical property of materials, which allows light to pass through the material without appreciable scattering of light. Haze, or the loss of transparency, is due to light scattering which can originate from both the interior of the film and from the film

surface. Roughness pores, and grain boundaries will scatter light, significantly comprising transparency.[47] For example, glass has no internal grain boundaries and few impurities, allowing most light to travel through, and hence it appears transparent. But if the several layers of the same glass are laid on top of each other, the transparency level will decrease significantly or totally be lost after grinding into powder as demonstrated in Figure 5a.

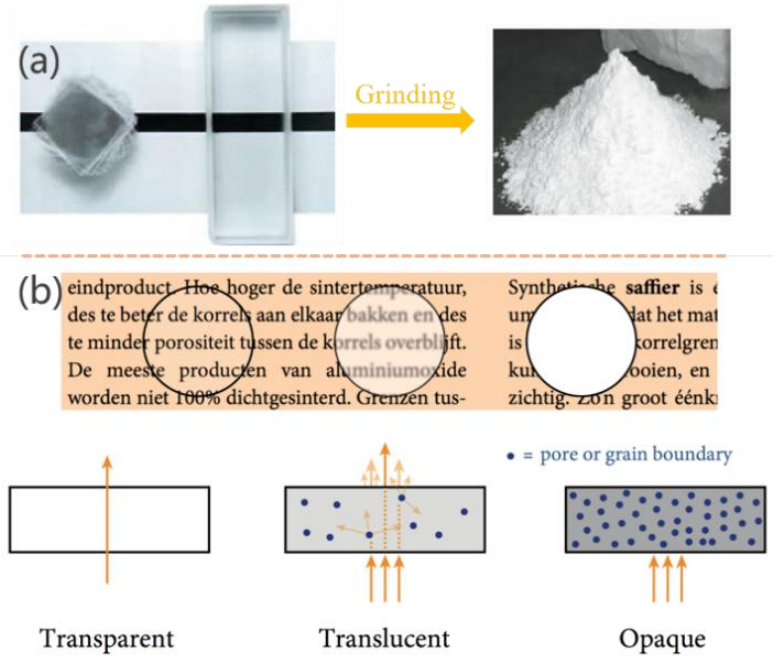


**Figure 5**. Transparency. Digital images of (a) layered glass slides, single glass slide, and after grinding into powder;[45] (b) illustration of material structure influence on their optical property.[46]

Figure 5b shows the influence of scattering centers quantity on the optical properties. Severe loss of transparency happens due to thousands times of reflection and scattering on the pores, grain boundaries, and impurity spots. In principle, high transparency in the visible region and superhydrophobic properties are mutually exclusive. Rough surfaces increase the water contact angle but decrease transparency accordingly.

Two theories, Raleigh scattering and Mie scattering, are often applied to study the scattering behavior of light. Both theories assume the surface roughness is created by spherical and non-absorbing particles that redirect the incident light. The relationship between particle size and incident light wavelength is used to categorize the scattering models. Rayleigh scattering occurs when the particle size is much smaller than the wavelength of the incident light ($<1/10\ \lambda$). Its effect is negligible in the visible light

region (400 nm ≤ λ ≤ 700nm). This obscure phenomenon caused by surface roughness is mainly due to the Mie scattering effect.[48] Mie scattering theory is described in the following equation:[49]

$$C_{SCA} \approx \frac{\pi d^2}{2} \sum_{n=1}^{\infty} (2n + 1)(a_n + b_n)$$

According to the theory, the scattering cross section ($C_{SCA}$) provides a quantification of light scattering as a function of particle diameter (d), where $a_n$ and $b_n$ are Mie coefficients of the order n, relating to the electromagnetic properties of the material. The $C_{SCA}$ is directly proportional to the square of the particle diameter (d), indicating the existence of an upper limit beyond which the surface feature size (i.e. roughness), while providing a platform for superhydrophobicity, will result in significant light scattering, and thus reduce transparency. Therefore, it is necessary to find the "critical window", where the roughness is optimized for transparency yet high enough for superhydrophobicity.[49] Based on research, surface roughness below the wavelength of incident light can help minimize Mie scattering. Sub-100nm, roughly less than one-quarter of the wavelength of visible light has been proved to be the sweet-spot that can allow for superhydrophobic surfaces with high visible light transparency.[33b, 50] Therefore, to some extent, both transparency and superhydrophobicity of the surfaces can be obtained simultaneously. However, the required micro/nanostructures for superhydrophobicity are usually vulnerable to abrasion. The intrinsic contradiction of transparency and superhydrophobicity plus durability issues are the major barriers for advancement.[51]

## 4. Fabrication of transparent and superhydrophobic surfaces

### 4.1 Typical Fabrication Processes and Materials

In general, there are two processes to fabricate transparent and superhydrophobic surfaces/coatings. One is to construct micro/nanostructures on the substrate, or any surface of interest first, followed by applying low-surface energy material coating. "Top-down" and "bottom-up" techniques can be used for fabricating the roughness required.[32a,52] Representative top- down approaches include laser ablation, etching, galvanic corrosion, and photolithography. In top-down fabrication, the rough structure is an integrated part of any substrates or bulk materials, and thus it has relatively high mechanical durability. The properties of the substrates or bulk materials are very crucial to the processability and quality of the surface. The low throughput and high cost of top-down approaches are the main limiting factors of their practical applications. Bottom-up approaches that grow micro/nano building blocks with various shape (e.g. nanowires, nanorods, spheres, flowers, etc.) is more cost-effective. [39, 51] Micro/nanostructures produced via bottom-up approaches are not originated from the substrates or bulk

materials, possibly leading to poor mechanical durability. Another process is to have a mixture of ingredients with each individual component contributing to required roughness and low surface energy. For example, various nanoscale ceramic powders and fluorine-based silane precursors are frequently blended together to coat on the surfaces of interest. The function of nanopowders is to generate the required roughness, and the fluorine-based silane is to reduce surface energy.[53] In terms of coating the solution mixture, frequently used methods include spraying coating, spin coating, and dip-coating.[54] These methods are simple and affordable for large surfaces, but they also face the durability challenges since the surfaces are externally grown on a substrate.

**Table 1.** Typical values for optical properties, electrical resistivity, and hardness for $SiO_2$, ZnO, and ITO.[56]

| particle | band gap energy (band gap wavelength) | refractive index | hardness (GPa) | electrical resistivity (Ω cm) | potential benefits |
|---|---|---|---|---|---|
| $SiO_2$ | 8.9 eV (138 nm) | 1.5 | 9 | $1 \times 10^{18}$ | high visible transparency, high hardness |
| ZnO | 3.3 eV (375 nm) | 2.0 | 5 | 28 | UV-protective effect |
| ITO | 3.6 eV (345 nm) | 1.8 | 7 | $2 \times 10^{-4}$ | transparent conducting oxide |

In terms of materials, polymers with fluorine groups are often used for surface modification because the $CF_2$ and $CF_3$ groups have the lowest surface tension out of many other molecular structures ($CH_2$ (36 dyn/cm) > $CH_3$ (30 dyn/cm) > $CF_2$ (23 dyn/cm) > $CF_3$ (15 dyn/cm)). For example, polytetra-fluoroethylene, commonly known as PTFE or Teflon, is composed of repeating $CF_2$ units and has a low surface energy (18.5 dyn/cm), showing high hydrophobicity and low wettability.[55] Nanoparticles are frequently added to obtain the structure roughness. One of the most widely adopted nanoparticles is $SiO_2$ due to the ease of synthesis (e.g. Stöber method) and good control of properties (e.g. size, hollow or solid structure, and functional surface modification). $SiO_2$ is also commercially available at very affordable price. Other oxides such as zinc oxide (ZnO) and indium titanium oxide (ITO) are also widely studied, both having high chemical and thermal stability, high hardness, high transmittance for visible light due to low refractive index (minimizing reflectance), and low cost. More importantly, the band gap wavelength is shorter than the visible range of 400-700 nm, helping to minimize visible-range absorption.[56] Additionally, $SiO_2$ has high visible transmittance. ZnO offers UV-protective and catalytic functions, and is able to mitigate photodegradation. Doping with other elements like Al or Ga, ZnO can also be used for transparent conducting films.

ITO is the most commonly used material for transparent conducting films due to its combination of high visible transmittance and low electrical resistivity. A brief summary of the properties of the mentioned oxides are available in Table 1.[56]

### 4.2 Representative Case Studies

There are many superhydrophobic and transparent surface reports available. [30, 32a, 33a, 39, 57] Thanks to the great effort of Ebert et al., two summary tables of recent studies in fabricating transparent superhydrophobic materials are also available.[56] To well-demonstrate the fabrication processes, several case studies based on different material selections (e.g. polymers, inorganics, polymer and inorganic composites) are presented and introduced in this paper as following.

#### 4.2.1 Polymeric surfaces

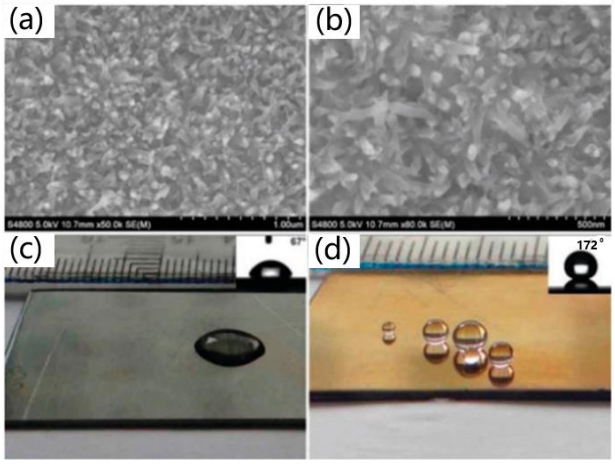


**Figure 6.** Polymer surfaces. SEM images of the transparent superhydrophobic coating on a stainless steel substrate at low (a) and high (b) magnifications, respectively. The optical images of water droplets on the substrates of a bare stainless steel (c) and the PANI-coated surface (d). The insert images in (c) and (d) are the respective contact angles. [58]

A robust, transparent, and anti-fingerprint superhydrophobic polymeric film was reported by Wang *et al.* [58] In this study, a polyaniline (PANI) nanofiber forest was first grown on stainless steel by a dilute chemical polymerization. Secondly, 1H,1H, 1H,1H–perfluorodecanethiol was coated on the rough forest for low surface energy, and thus obtained the superhydrophobic property. The coating shows the characteristic green color of PANI and is highly transparent. By precisely controlling the reaction times, the final superhydrophobicity as well as the transparency can be optimized. As can be seen in Figure 6 a and b, the PANI nanofibers are aligned perpendicularly and can fully and

uniformly cover the substrate surfaces. The superhydrophobic property of stainless steels with and without PANI nanofibers are demonstrated in Figure 6c and d. Bare stainless steel has a contact angle of approximately 67° measured with a 5 µl of water droplet, showing hydrophilicity, while water droplets on the PANI-coated surface after modification resemble a sphere and the contact angle reaching as high as 172° with sliding angle close to 0°, showing super water-repellency at a very low contact angle hysteresis. In comparison to the bare stainless steel, the coated surface also shows enhanced anti-fingerprint performance of about 80–85%. This coating can be grown on a wide range of conducting and non-conducting substrates.

In another work, a hydrophobic polytetrafluoroethylene (PTFE) thin film was deposited on a glass substrate by pulsed laser deposition method and exhibited a contact angle of around 151.6°. UV-vis spectroscopic analysis of the PTFE films revealed that they were highly transparent, up to approximately 90% in visible and near infrared ranges.[55]

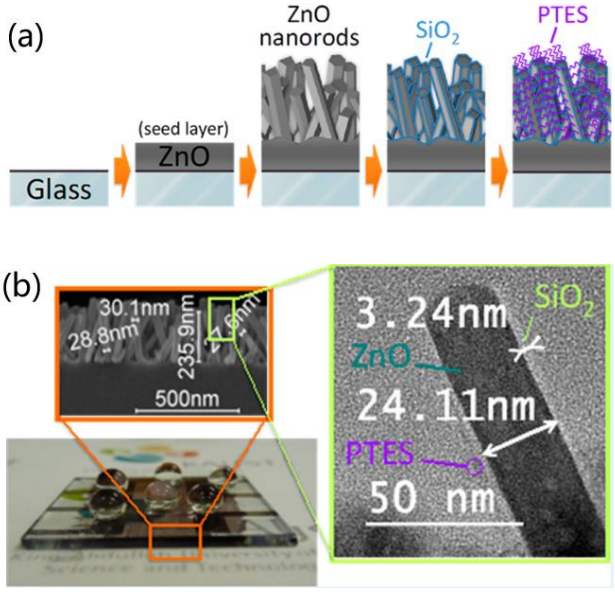


**4.2.2 Inorganic surfaces**

**Figure 7.** Inorganic surfaces. (a) Schematic description of the preparation of superhydrophobic $SiO_2$-coated ZnO nanorod arrays on glass (PTES = perfluorodecyltriethoxysilane) (b) Digital picture of water droplets on the coated glass, SEM image of cross-section of ZnO nanorods obtained after 25min deposition, and TEM image of $SiO_2$-coated ZnO obtained after 3h of $SiO_2$ deposition. [59]

Highly transparent and UV-resistant superhydrophobic arrays of $SiO_2$ coated ZnO nanorods were prepared in a sequence of steps shown in Figure 7. The length of ZnO

nanorods and thickness of $SiO_2$ layer are very influential for the superhydropbhocicity. The coating can be deposited on both glass and flexible thin PET sheets, having a contact angle of 157° and 160°, respectively. It is very robust and invariant even after repeated bending (coating on PET). The film is also highly transmissive (avg. 93-95%) and UV-resistant. When deposited on solar cell panel, the superhydrophobic $SiO_2$/ZnO nanocomposite coating showed minimal impact on solar cell device performance.[59]

Yadav *et al.* studied the influence of indium oxide nanorods alignment on the surface properties. They synthesized randomly distributed and vertically aligned indium oxide nanorods via chemical vapor deposition method. It was found that the static water contact angle shows a significant dependence on the alignment of the nanorods. The randomly distributed nanorods shows the value of 133.7° ± 6.8°. While the contact angle is 159.3° ± 4.8° for vertically aligned indium oxide nanorods.[60]

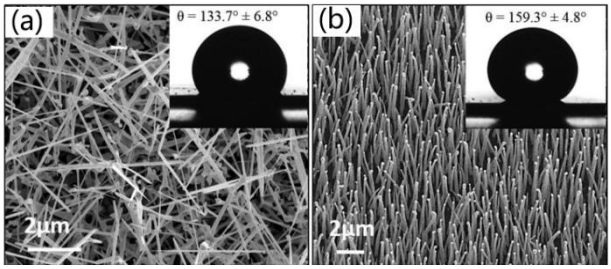


**Figure 8.** FESEM images of (a) randomly distributed and (b) vertically aligned indium oxide nanorods. The insets show the contact angle images of the respective samples.[60]

Oak Ridge National Laborataries demonstrated the formation of low-refractive index, antireflective, superhydrophobic glass films that embody omni-directional optical properties over a wide range of wavelengths. The fabrication process is shown in Figure 9a-d. Magnetron sputtering was used to deposit the nanostructured glass coating. During post-thermal treatment, the glass coating phase was separated into an interpenetrating pattern consisting of alkali-borate-rich and a silica-rich phases, with the former being relatively more soluble by a variety of chemicals. In the following step, selective etching is employed to dissolve the sodium-borate-rich phase, leaving behind an interconnected, porous, and three-dimensional reticulated network of high-silica content glass phase (Figure 9e). Simply changing the surface chemistry with low surface energy functional groups of 1H,1H,2H,2H-perfluorooctyltrichlorosilane, the coatings show exceptional superhydrophobicity with the static water droplets' contact angle value as high as 165°. The water droplets on these surfaces assume to have spherical shapes (Figure 9f) and roll

off very easily at a tilt angle less than 5°. When $Al_2O_3$ is used to simulate the outdoor sand/dust-storm conditions (rather than much softer and more natural $SiO_2$), the coating surface still demonstrates self-cleaning ability of the coating (the inset of Figure 9f). This approach enables well patterned surface microstructures with graded-index antireflection characteristics, where the surface reflection is suppressed through optical impedance matching between interfaces. Based on near complete elimination of Fresnel reflections, it yields more than 95% transmission through a single-side coated glass. Moreover, these antireflective surfaces demonstrate superior resistance against mechanical wear and abrasion.[61]

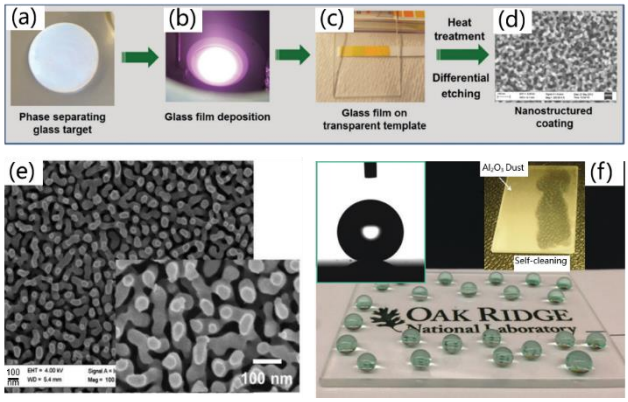


**Figure 9.** Preparation of nanostructured silica films. (a) sputtering target, (b) deposition during magnetron sputtering, (c) photograph of the sputter-coated glass substrate, (d) SEM image showing the nanostructured surface morphology of the coating after the post-deposition treatments (scale bar:100 nm), (e) SEM images of fully processed, phase separating glass films on fused silica substrates with 120 min heat treatment time at 710° C, (f) Photograph of blue dyed water droplets on a borosilicate substrate coated with nanoporous antireflective glass film. The film surface is modified by a covalently bonded organosilane chemistry. Inset shows the profile of a 5 ml water droplet resting on a similarly processed film, the inset is appearance of the sample after the impact abrasion test with $Al_2O_3$ particles. [61]

Coatings that are simultaneously superhydrophobic and superoleophobic are rare. Deng et al. designed an easily fabricated, transparent, and oil-rebounding superamphiphobic coating.[62] In their work, a porous deposit of candle soot was used as template (Figure 10a, b, and c) and coated with a 25- nanometer-thick silica shell (Figure 10d). The black coating became transparent after calcination at 600 °C (Figure 10e and f). A water drop placed on top of the coating formed a static contact angle of 165°± 1° with a roll-off angle lower than 1° (Figure 10g). A list of organic liquids were also tested, and the data is shown in Table 2. The static contact angles ranged from 154° for tetradecane, 156° for

hexadecane (Figure 10g), and up to 162° for diiodomethane. Figure 10i shows the digital pictures of different liquid droplets on the coating. The possible liquid-interface schematic illustration on the fractallike surface is shown in Figure 10h. The coating is very robust, which remains superamphiphobic even after its top layer was damaged by sand impingement.

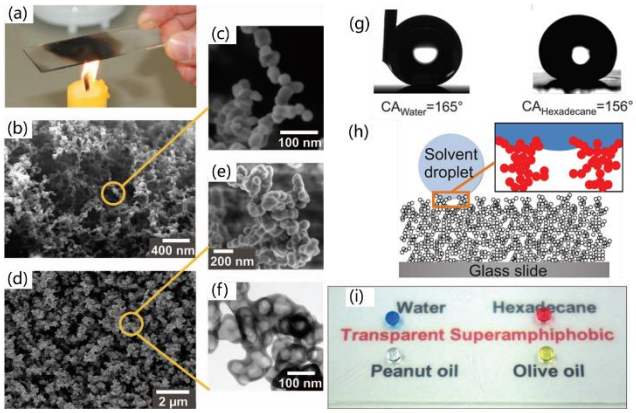


**Figure 10**. Morphology of porous structure. (a) Photograph depicting sample preparation. A glass slide is held in the flame of a candle until a soot layer a few micrometers thick is deposited. (b) SEM image of the soot deposit. (c) High-resolution SEM image showing a single particle chain made up of almost spherical carbon beads 40 ± 10 nm in diameter. (d) SEM image of the deposit after being coated with a silica shell. (e) High-resolution SEM image of a cluster after the carbon core was removed by heating for 2 hours at 600°C. (f) High-resolution TEM image of a cluster after calcination, revealing the silica coating with holes that were previously filled with carbon particles. (g)Contact angle of water and hexadecane. (h) Schematic illustration of a liquid drop deposited on the fractal-like composite interface. (i)Digital picture of different liquid drops on the coating surface.[62]

**Table 2.** Comparison of the static contact angle (SCA) and roll-off angle of drops with different surface tension, deposited on a flat fluorinated glass substrate and on a superamphiphobic coating.[62]

| Liquid | Surface tension (mN/m) | Flat surface SCA° | Superamphiphobic surface SCA° | Roll-off angle° |
|---|---|---|---|---|
| Water | 72.1 | 108 ± 1 | 165 ± 1 | 1 ± 1 |
| Diiodomethane | 50.9 | 91 ± 1 | 161 ± 1 | 2 ± 1 |
| Ethylene glycol | 47.3 | 89 ± 1 | 160 ± 1 | 2 ± 1 |
| Peanut oil | 34.5 | 70 ± 1 | 158 ± 1 | 4 ± 1 |
| Olive oil | 32.0 | 69 ± 1 | 157 ± 1 | 4 ± 1 |
| Hexadecane | 27.5 | 64 ± 1 | 156 ± 1 | 5 ± 1 |
| Tetradecane | 26.5 | 54 ± 1 | 154 ± 1 | 5 ± 1 |

### 4.2.3 Polymer-inorganic surfaces

Polymer-inorganic surfaces are usually coated with a pre-prepared solution mixture of inorganics and organics. For example, Li *et al*. designed and fabricated a transparent, durable, and self-cleaning superhydrophobic coating using a trimethoxypropylsilanesilica nanoparticles sol solution. For the preparation of coating solution, $SiO_2$ was first dispersed in ethanol and then trimethoxypropylsilane (PTMS) was added dropwise at room temperature. The modification of $SiO_2$ is based on the reacting characteristics of trimethoxypropylsilane as shown by the equations in Figure 11a. The final modified solution is then sprayed on substrates to form superhydrophobic coatings with high transparency. The coating process and digital image of the coated surface is shown in Figure 11b. It has high water contact angle of 158.5° as well as low sliding angle of 3.9°. The transmittance of the coated glass substrates is above 80% in the visible-light region (400-800nm).[53b] It should be noted that no fluorinated functional groups is involved in this process, which can potentially reduce cost and be more environmentally friendly.

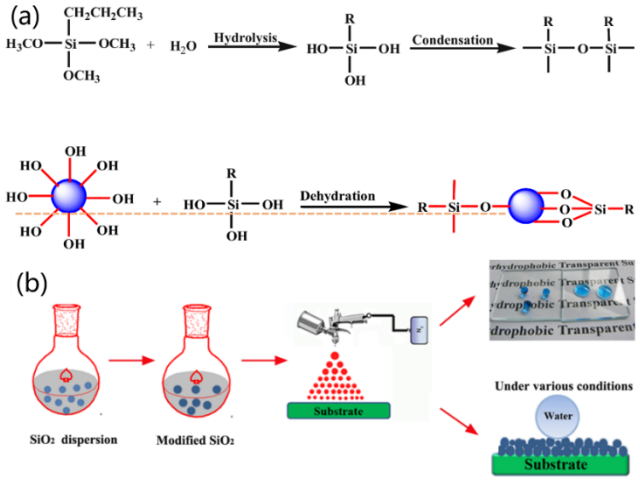


**Figure 11.** Schematic illustration of (a) $SiO_2$ modification process and (b) the fabrication of nonfluorinated superhydrophobic coatings with high transparency.[53b]

Great effort has been made on fluorine-free coating since fluorinated composition is known to be very expensive and can cause severe environmental issues. Mates et al. developed an entirely water-based and fluorine-free superhydrophobic formulation from hydrophilic titanium dioxide ($TiO_2$) nanoparticles and polyolefin copolymers without additional surfactants or charge stabilization, serving as a promising environmentally-safe functional coating method.[63] Recently, Chen et al. developed a facile, economical, efficient strategy for environmentally friendly, mechanically robust, and transparent superhydrophobic surfaces. All the ingredients they used are commercially available,

including adhesive 75 from 3 M Co. Ltd. and $SiO_2$ nanoparticles modified with dimethyldichlorosilane (AEROSIL R972 from Degussa, German). To make the surface, adhesive 75 was sprayed for 3 s on any interesting surfaces of different substrates (e. g. steel mesh, glass slides, PU sponge, and silicon wafer), then the modified $SiO_2$ suspension was sprayed on the adhesive-modified substrates for 6 seconds. Simply repeating the spraying cycles, a ferroconcrete-structured superhydrophobic coating on the substrate can be obtained after drying in air for 5 minutes. The fabrication process is demonstrated in Figure 12. The water droplets stayed in spherical shape on the as-prepared glass slide with a WCA of ~160°. The coated glass slide with six spraying cycles retained its superhydrophobic property (WCA>150° and SA < 10°) even after 325 abrasion cycles with sandpaper, displaying great mechanical abrasion resistance. They also coated sponges with the adhesive and modified $SiO_2$, which showed great water/oil separation performance. In short, it is a very simple and scalable process that is suitable for many practical applications.[64] Future development will continue focusing on cost-effective, environmentally friendly, and scalable recipes and approaches for various applications of superhydrophobic films.

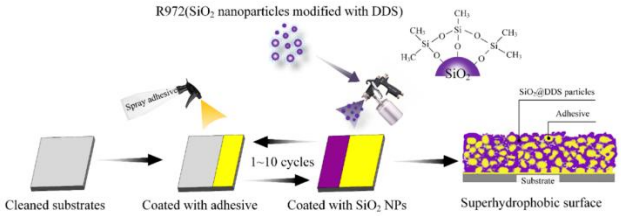


**Figure 12.** Schematic illustration of the fabrication procedure of the superhydrophobic surface.[64]

### 4.2.4. Mechanically Robust Structure Design

The structure roughness required to minimize contact area between liquid and solid are usually fragile and susceptible to abrasion wear, shear, and ice adhesion. It is important to develop coating that is mechanically durable in order to have any practical applications. Otherwise, the loss of nanoscale roughness will lead to a rapid decrease of WCA and the increase of sliding angles.[65] Various approaches have been explored to address this issue, including bond strengthening between the coating layer and substrate, bearing the abrasion force by randomly introducing discrete microstructures, and allowing abrasion by sacrificing the upper layers of a selfsimilar structure.[31, 62] Yokoi et al. fabricated a highly transparent and superhydrophobic thin film with enhanced mechanical abrasion

resistance by combining a see-through hydrophobic mesh with a hydrophobic $SiO_2$ nanoparticle hierarchical structure. After 100 cycles of abrasion under a pressure of approximately 10 kPa, the water contact angle and the water sliding angle remain greater than 150° and lower than 25°, respectively, and the transmittance remains approximately 79%. Very recently, Wang et al. realized robust superhydrophobicity by structuring surfaces with two different length scales, a nanostructure designed to provide water repellency and a microstructure design to provide durability.[31]

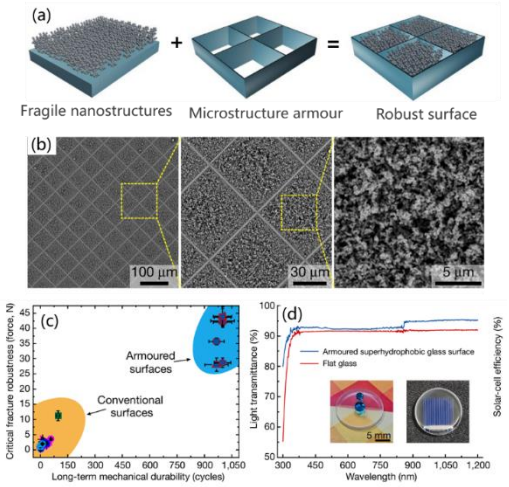


**Figure 13.** Mechanically robust structure design. (a)Schematic images showing the strategy for enhancing the mechanical stability of the superhydrophobic surface by housing water-repellent nanostructures within a protective microstructure 'armour', (b)SEM images of silica fractal nanostructures housed within the silicon microstructure frame after abrasion, (c)Comparison of the mechanical stabilities of different superhydrophobic surfaces, (d) Transmission spectra of armoured glass (blue) fabricated using a flat glass substrate (red). The photographs show the transparency and the superhydrophobicity of the armoured glass substrate (left) and a solar cell assembled with an armoured glass superhydrophobic surface as the cover plate (right).[31h]

The microstructure with an interconnected surface frame containing 'pockets' is to house highly water-repellent and mechanically fragile nanostructures, acting as 'armour' to prevent the removal of the nanostructures by abradants that are larger than the frame size. The schematic illustration of the intentionally designed structure and SEM images after abrasion are shown in Figure 13a and b, respectively. It was also tested that the designed coating can tolerate more than 1,000 abrasion cycles, which is 10 times higher than that of the conventional superhydrophobic surfaces (Figure 13c). This strategy is applicable

on various substrates including silicon, ceramic, metal and transparent glass. Also, the water repellency of the resulting superhydrophobic surfaces is preserved even after abrasion by sandpaper and by a sharp steel blade. The optical transparency of the coating is very high (Figure 13d). Upon coating on solar cell, it helps maintain high energy conversion efficiency through the passive removal of dust contamination, which could potentially lead to large savings in terms of freshwater, labor and cost compared to the traditional cleaning processes. The generality and effectiveness of this design principle could greatly guide the superhydrophobic surfaces research and study.

## 5. Summary and outlook

In this contribution, we first briefly introduced the significance of developing superhydrophobic and transparent surfaces for various practical applications. Secondly, fundamentals of superhydrobphobicity and different wetting models were presented. Inspired by natural phenomena, the requirements of superhydrophobic surface construction were listed and discussed. Thirdly, the fundamentals, key governing factors for transparency, and the conflicting relationships between superhydrophobicity and transparency were introduced. After the theoretical discussion, experimental design and methods were summarized and representative case studies were briefed. The review is expected to offer readers a quick understanding of the focused research area and inspire new research development. Several aspects are proposed for future effort in the discussed topic. Although there is a large pool of research works, there is a lack of universal testing procedures/protocols for performance evaluating. For example, the mechanical durability and abrasion test procedure profoundly varies in reports. Sand-paper gritting, sand impact setup, rotary platform abrasion and the likes were used, making the cross literature comparison difficult. In terms of the surface design, recent development in computer simulation can help optimize the surface structure and balance the conditions, especially roughness for both superhydrophobicity and transparency, which will greatly guide the experimentalists' work and significantly reduce time and cost. On the experimental side, non-fluorine materials with low-cost and environmental friendliness are desired. Surfaces with strong mechanical robustness and wide applicability on various substrates are crucial for long lasting coating applications. Methods with wide adaptability, fast surface coating, and high-quality coating are required for large area applications. In conclusion, this introductory review will help the research community better understand this type of surface and further accelerate the development of potential artificial coating materials for innovative applications.

# Objective

Primary objective of this report was to introduce a facile method of fabricating superhydrophobic coating on transparent surfaces. In this report, a mixture of silicon dioxide nanopowders and polyacrylonitrile/n,n-dimethylformamide solution was used to test the new method and assess its potential for surface coating applications. The process parameters involved including concentration, air flow rate, solution infused rate, and power voltage were thoroughly investigated. Further, different methods such as blading and dip coating were demonstrated for the better comparison of the quality and water repellent behavior of coatings. The wettability behavior of the surfaces was analyzed with contact angle measurement and correlated with the surface structures.

# Scope

The results of this report could lead to the potential use in various industrial applications of self-cleaning and anti-corrosion surfaces. A series of tests consisting of sandpaper abrasion, tape peeling test, anti-acid/base, and outdoor exposure examination were conducted to examine the reliability of the coating against harsh environmental conditions.

# Methodology

**1. Materials**

Microscope glass slides (high-quality soda-lime glass, 3 in × 1 in, with ground edges and frosted on one end, 90-degree corners) were acquired from Karter Scientific. Polyacrylonitrile (PAN, with average Mw 150,000), Silicon dioxide ($SiO_2$, spherical porous nano-powder, 5-20 nm particle size, 99.5% trace metals basis), and Trichloro (1H,1H,2H,2H-perfluorooctyl) silane (97%) were sourced from Sigma-Aldrich Corporation (St. Louis, Mo). N,N-Dimethylformamide (DMF), Acetone (ACS reagent, ≥99.5%), and Ethanol (96%, anhydrous) were purchased from VWR Chemicals. Carbon black (C65) was provided by Gelon Lib Group. Hydrochloric acid solution (1M HCl) and sodium hydroxide solution (1M NaOH) were obtained from Sigma-Aldrich. All chemicals were used without further purification. Deionized water purified in an ultrapure water system was used in all experiments.

**2. Preparation of the superhydrophobic coatings**

The spraying solution was prepared by first adding a predetermined amount of PAN (varying from 0 mg to 200 mg) in 5mL of DMF, then storing in an oven overnight at 70ºC to obtain the PAN-DMF solution. $SiO_2$ nanoparticles were dispersed in PAN-DMF solution at room temperature with different concentrations ranging from 50 mg to 300 mg. The solution was then ultrasonicated for 3 hours and stirred magnetically with constant speed of 400 rpm for 24 hours. Glass substrates were washed with ethanol, acetone, and deionized water for at least 3 times. They were then ultrasonicated for 30 minutes and dried at room condition for 2 hours prior to coating on the substrates.
The prepared solution was deposited on the cleaned glass slides via electrospray method at different voltage (range from 0 to 20 kV) under room condition. Coaxial needles were used for electrospraying, where the solution was introduced through the inner needle (17 gauge) and air was injected to the outer needle at the flowrate of 2, 3, 4, 5, and 6 L/min. The solution infused rates (10, 20, 30, 40, and 50 μL/min) and spray periods (0.25, 0.5, 0.75, 1, 1.5, 2, and 2.5 hours) were set at predetermined values for different samples which were later characterized and optimized. Walfront LZQ-7 acrylic air flowmeter was used to control the air flowrates.

Coated glass substrates were stored overnight at room temperature. They were annealed in air at 600ºC for 90 mins, and then modified with low surface energy trichloro (1H,1H,2H,2H-perfluorooctyl) silane via chemical vapor deposition technique. The

coated glass slides and an open glass vessel containing 40μL of trichloro (1H,1H,2H,2H-perfluorooctyl) silane were placed in a homemade sealed pot for 5 minutes at a high vacuum condition and at room temperature. Afterwards, the open glass vessel was then removed from the sealed pot, and the coated substrates themselves were sealed in the pot for 30 mins at 80ºC to remove untreated silane residues.

**3. Characterizations and measurements**

**3.1. Wetting test.** Drop shape analyzer DSA 100 apparatus from KRUSS company, Ltd., Germany was used to measure static water contact angle (WCA) of the coating at various air flowrates (2, 3, 4, 5, and 6 L/min). Water droplets with the volume of 2μL to 3 μL consistently were deposited on the coated substrates. Static images of the droplets on the surfaces were captured and WCA data was collected by the apparatus. Contact angle measurements were taken at standard temperature and pressure.

**3.2. Surface morphology.** Scanning electron microscopy (SEM, Scios 2 DualBeam) was used to investigate the morphologies and the thickness of the superhydrophobic coatings. Before generating images captured by SEM, all samples were gold-sputtered under high vacuum condition with a sputter coater to improve the electrical conductivity of the coatings.

**3.3. Transparency.** The transparency of the most superhydrophobic surface was measured using the ultraviolet-visible (UV-Vis) transmittance spectrum (Agilent Technologies). Air was used as the blank. The percentage of transmittance over the wavelength range of 200-800 nm of the origin pristine glass slide versus the coated surface were obtained from the UV-Vis apparatus.

**3.4. Self-cleaning examination.** The self-cleaning functionality of the coatings was experimented with carbon black particles sprinkled on the sample's surface. The substrate was placed at an angle of 20º to the flat table surface. Deionized water was continuously injected to the surface. The self-cleaning capability was tested based on the ability of water droplets rinsing off the surface with carbon black particles. Additionally, the experiment of a water droplet picking up carbon black particles on the coated surface was performed. Black and white images and videos of the self-cleaning examination were also captured using the drop shape analyzer DSA 100 apparatus.

**3.5. Durability of the coated layers.**

To assess durability, sandpaper abrasion, tape adhesion test, anti-acid/base test, and outdoor exposure examination were performed.

**3.5.1. Sand abrasion test.** The sandpaper of grit 400 was used to examine the abrasion analysis. The coated glass slides were placed face down onto the surface. 100g glass vessel of sand was place on top of the coated substrates. The substrates were reciprocally moved with a round trip distance of 10 cm. The above round trip was referred as one abrasion cycle. The WCA measurements of the coating before and after abrasion cycles were obtained for analyzing.

**3.5.2. Tape adhesion test.** The 3M doubled side tape was used to perform the adhesion test. The coated glass slide was stably placed on aluminum sheet with coating surface facing up. The tape was attached to the coated surface, scratched, and then peeled off, which referred as one cycle. WCA measurements were performed before and after peeling cycles to evaluate the superhydrophobic property of the coatings.

**3.5.3. Anti-acid/base test.** Two coated glass slides were separately immersed into two beakers containing 150 mL 1M HCl and 1M NaOH overnight. Afterwards, the coated glass slides were dried in air under room condition for one day. WCA measurement of the coated surface before and after being immersed in acid and base solution were obtained. An additional experiment to rinse off the coated surface with DI water after acid/base tests followed by drying in air at room temperature was conducted as well.

**3.5.4. Outdoor exposure test.** The coated glass slide was placed outside for 15 days, and static water contact angle measurement was obtained every 3 days for analysis.

# Discussion of Results

In this report, superhydrophobic surfaces were obtained via air-assisted electrospray, followed by thermal treatment and chemical vapor deposition (CVD) techniques as shown in Figure 14. The air-assisted electrospray tends to accelerate the drying of deposition process by utilizing a convective air flow jet. The nozzle is comprised of two concentric cylindrical needles. The silicon dioxide ($SiO_2$) nano-powders in the polyacrylonitrile and dimethylformamide (PAN-DMF) solution were deposited to the substrate through the inner needle with the assistance of air through the outer needle for the air-assisted electrospray process. To be specific, the air helps atomize the big solution droplets into small ones so that electrostatic force is able to bring them to target. Similar to electrospinning, solvent can be simultaneously evaporated during the process. This electrospray process is carried out at a high voltage condition. Using this method for electrode preparation, Halim et al. indicated that the dry solute is deposited on the substrate because smaller charged droplets are formed and solvent is evaporated faster via the assisting of the impinging dry air.[66] Wet solutions formed on the substrate may disrupt the uniformity with low evaporation rate as the solute may migrate and agglomerate on substrate upon solvent evaporation, whereas, solute may form discontinuity and disorder of the deposited materials with fast evaporation rate.[66] To achieve the optimal evaporation rate during the air-assisted electrospraying process so that good control on structure, different parameters consisting of power supply voltage, sprayed time, solution infused rate, and air flowrate are examined in this study. In addition, variety of PAN and $SiO_2$ concentration in DMF solution are tested to determine the effect of sprayed solution on the superhydrophobic property of the coating. Thermal treatment and chemical vapor deposition steps were indicated in the schematic with corresponding conditions remaining unchanged for all testing samples.

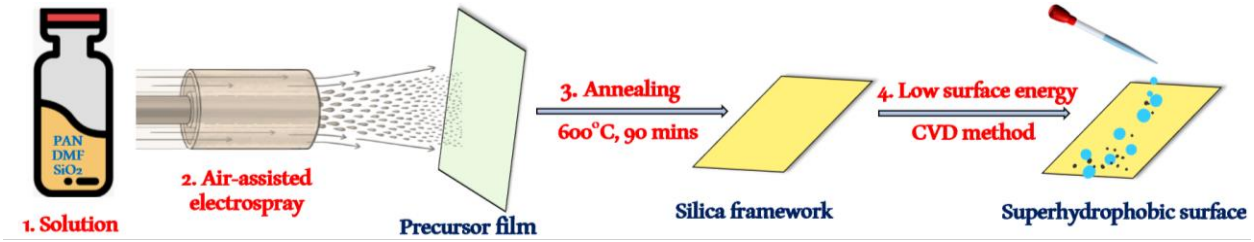


**Figure 14.** Schematic diagram of the fabrication process of superhydrophobic surface on glass substrate

### 1. Method comparison

For comparison, dip coating and blading coating were also examined with the same precursor solution used in the electrospray. The static water contact angles of the coatings through the three methods are shown in Figure 15.

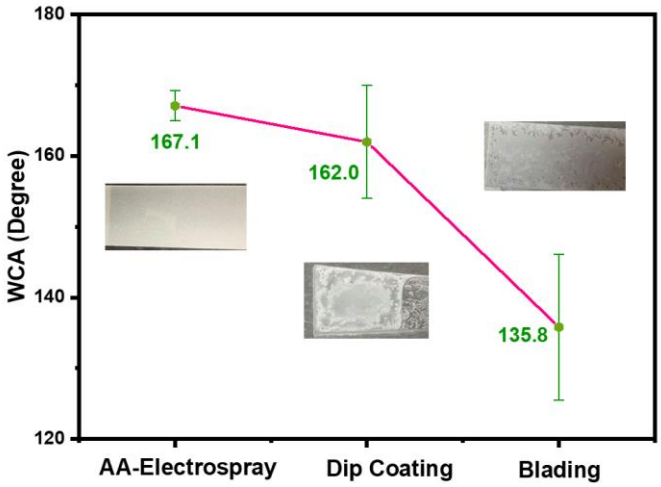


**Figure 15.** Comparison of three methods: Air-assisted electrospray (AA-Electrospray), dip coating, and blading.

The air-assisted electrospray results in the highest WCA of 167.1° with the smallest standard deviation. The WCA of 167.1° was obtained at 200mg of $SiO_2$, 50mg of PAN, 1 hour of spraying time, 20kV of power supply, 30 μL/min solution infused rate, and 3 L/min of air flowrate. The electrosprayed sample also shows excellent uniformity of the coating on glass substrate. Superhydrophobic surface is also obtained by dip coating method, however, after letting it dry in air, the coating cracked which affected the uniformity of the material distribution. Blading does not achieve superhydrophobic property, as shown in WCA measurement of 135.8° with very large standard deviation due to cracking occur on the surface. Hence, air-assisted electrospray is highly advantageous for the facile fabrication of superhydrophobic coating. Moreover, large surface area deposition can be achieved by multi-nozzle system and adjusted by nozzle number. The thickness of deposited layer and loading can be controlled by time variable.[24] In the following sections, various parameters will be studied for better understanding of the system.

**2. Effect of $SiO_2$ nanoparticles**

In the experimental design, $SiO_2$ is used to control the surface roughness. Various amounts of $SiO_2$ nanoparticles in the spray solution, including 50, 150, 200, and 250 mg, were used to study the effect of $SiO_2$ on wettability of coated surfaces. For simplicity, the surfaces are denoted of as SO-50, SO-150, SO-200, and SO-250, respectively. Each WCA

data point represents the average of five measurements at different locations of the samples. The WCA data and SEM images, as shown in Figure 16, confirm that the amount $SiO_2$ nano-powder significantly affects the superhydrophobicity and morphology of the coatings. The water droplet at SO-50 shows low contact angle where the surface's superhydrophobicity is not obtained. The SEM image of this sample (Figure 16b) confirms the coating after heat treatment is inadequate to cover a whole surface. Therefore, the roughness level of this sample is too low to obtain superhydrophobic surface. At 100 mg of $SiO_2$, the coated surfaces begin to achieve superhydrophobic properties, where WCA is greater than 150º. The WCA increases as the amount of $SiO_2$ increases until it obtains the highest measurement of 170.5º at SO-200. After SO-200, WCA decreases but still maintains superhydrophobicity. A small error bar at data point represents the uniform distribution of the coating, whereas a large error bar indicates higher variation in WCA measurements at different spots of the coating. The error bars illustration shows that at less than SO-200, electrospray results in uniform coating distribution. After SO-200, the sprayed solution was deposited unevenly on the surfaces resulting in a higher gap between the minimum and maximum measured values at the same sample. From the SEM images in Figure 16, the coating is getting denser as the amount of $SiO_2$ increases from SO-150 to SO-200. Compared to SO-200, SO-250 has less coating on the surface, possibly due to lower adhesion between the coating and substrate at SO-250. Therefore, most parts of the coating are easily removed after annealing at 600ºC in air. It is concluded that 200 mg is the optimal amount of $SiO_2$ which can result in very good coverage and highest WCA.

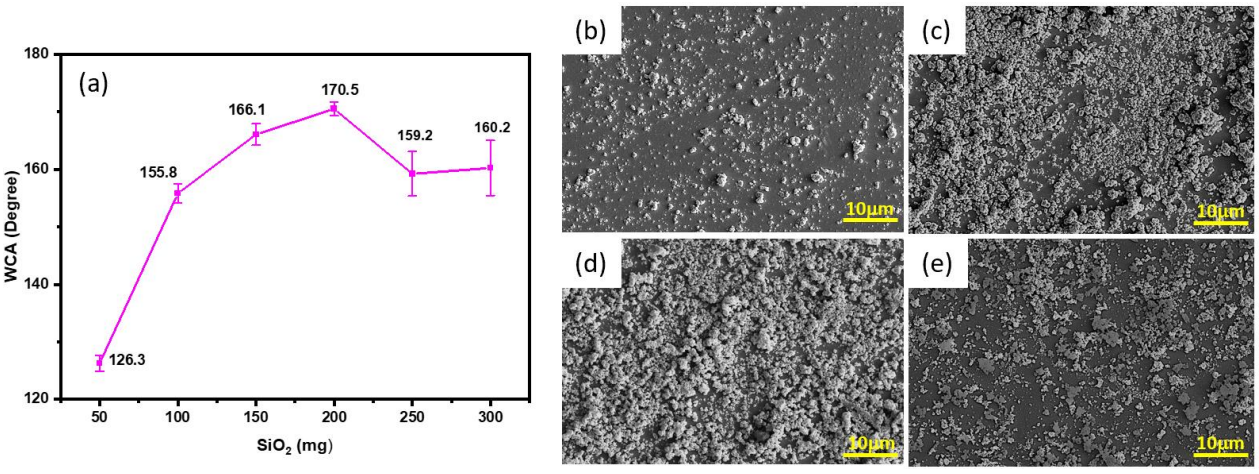


**Figure 16.** Effect of $SiO_2$ nanoparticles. (a) Water contact angle (WCA) vs amount of $SiO_2$ nanoparticles in the sprayed solution. Each data point represents n = 5 measurements, and the lower and upper error values represent the minimum and

maximum measured values, respectively. SEM images of (b) SO-50, (c) SO-150, (d) SO-200, and (e) SO-250.

**3. Effect of polyacrylonitrile (PAN)**

PAN in the solution serves two purposes. One is to increase the viscosity and help $SiO_2$ well disperse in the precursor solution rather than precipitate out, the other is to better guide the droplets spray and better adhesion on the substrate. As shown in Figure 17, the WCA of solution without PAN is 161.0º. With the presence of 50 mg PAN in the sprayed solution, the superhydrophobicity of the coating increases, demonstrated by its WCA of 169.1 º. Even though the CA measurements do not show significant differences when adding a small amount of PAN, the distribution of coating on the substrate's surface is more even, which is confirmed by the magnitude of the standard deviations of 0 mg and 50 mg PAN samples. Increasing amount of PAN is expected to increase superhydrophobic behavior of the coatings. However, WCA data starts decreasing dramatically after adding more PAN in the solution. The wettability of the coating changes from superhydrophobic to hydrophobic when the amount of PAN increases to 150mg. At 200mg PAN, the coating no longer obtained anti-wetting behavior in which its CA is 127.9º.

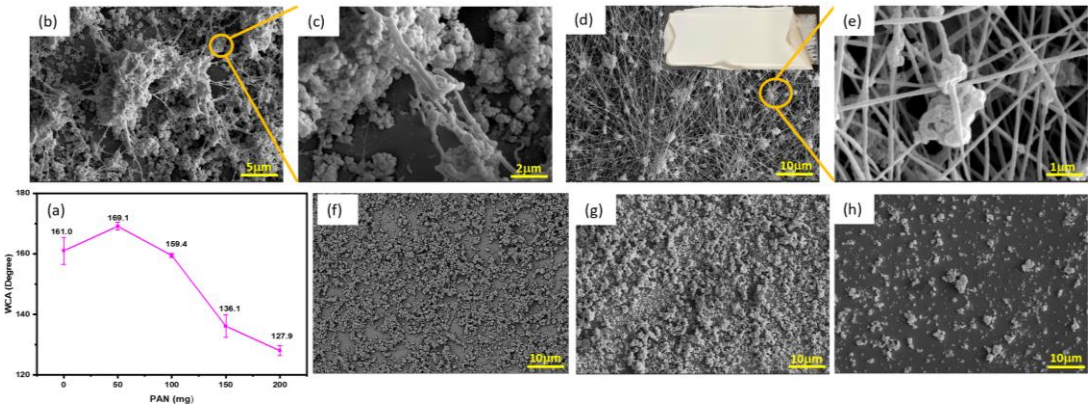


**Figure 17.** Effect of PAN. (a) The relation between WCA of coated surfaces at various amount PAN in sprayed solutions. SEM images of sample after electrospraying of (b,c) 50 mg PAN (d,e) 200 mg PAN, the inset image showing fiber layer peeling off of the glass's surface; and after completing fabrication process (annealing and CVD) of (f) 0 mg PAN (g) 50 mg PAN (h) 200 mg PAN.

Figure 17b-e show the SEM images of the coating after electrospraying. At this stage, thermal treatment has not yet been applied on the coating. Comparing the SEM images at 50 mg PAN (Figure 17b,c) to the images at 200 mg PAN (Figure 17d,e), the higher

amount of PAN results in denser fiber structure. As seen in the magnified SEM image of Figure 17c, the deposited layers possessed few fibers among $SiO_2$ depositions, whereas fiber structure is prevailed in Figure 17e. When the coating becomes fiber, it easily peels off the surface which leads to low adhesion, shown in the inserted images of Figure 17d. After heat treatment at high temperature (600$^{o}$C), PAN in the coating is burned out. Therefore, the distribution of the spray on the surface with high amount of PAN (e.g., 150 mg and 200 mg PAN) is uneven which results in higher standard deviation on WCA measurements on different location of the surface. Figure 17f-h represent the surfaces after completing fabrication process at 0, 50, and 200 mg PAN, respectively. From the coating density comparison, 50mg PAN results in better coverage and the best superhydrophobic behavior. In addition, the coating is wiped off significantly at 200mg PAN after thermal process.

**4. Effect of solution infused rate**

At the same materials' concentration, the relationship between WCA and solution infused rate, from 10 to 50 μL/min was shown in Figure 18a. With the increasing of solution infused rate, the water contact angles first increase and then decrease. When the infused rate is 30 μL/min, the WCA reaches the maximum values of 172.5$^{o}$, so the solution infused rate for the air-assisted electrospray process is selected to be 30 μL/min. With the increase of the infused rate, the coating on substrate was generated to be thicker, resulting in denser micro/nano rough structure. This rough structure, shown in Figure 18c, is more uniform than the structure at the solution infused rate of 10 μL/min (Figure 18b). The WCA starts decreasing significantly at the infused rate higher than 40 μL/min, however, the surface's superhydrophobicity is still maintained. Figure 18d is the SEM image of the surface at 50 μL/min. When the infused rate is too high, it wets the center area of the surface, as describe in the inserted images of Figure 18d. This wetted area, after annealing process at 600$^{o}$C for 1 hour, leaves a thinner layer of the coating comparing to outer area which is not wetted while spraying, indicating the simultaneous evaporation of solvent is crucial for coating uniformity and structure control. Thus, the superhydrophobicity decreases due to the reduction in coating thickness after annealing the wetted spot of the surface.

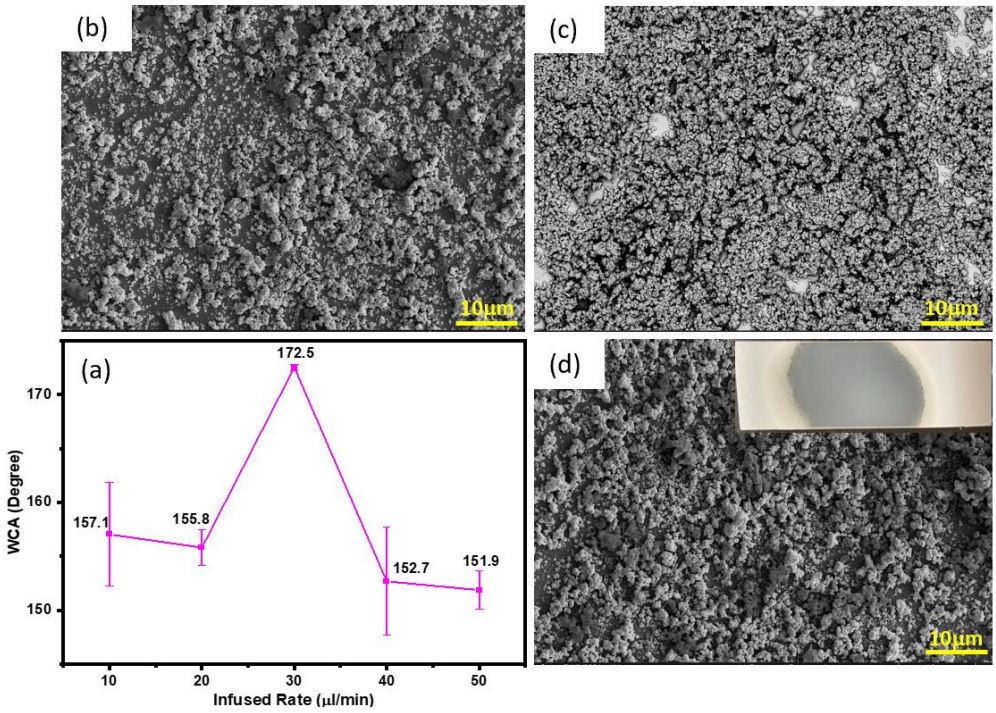


**Figure 18.** Effect of solution infused rate. (a) WCA of the coated layers on glass substrates at different solution infused rate. SEM images of coated surface of the solution infused rate at (b) 10 μl/min, (c) 30 μl/min, and (d) 50 μl/min (Inserted image of wetting spot of coated surface after electrospraying at the infused rate of 50 μl/min).

**5. Effect of sprayed voltage**

To evaluate the voltage effect on the superhydrophobicity of the coatings, different voltage conditions were examined, as shown in Figure 19a. Voltages were used at 0, 5, 10, 15, and 20 kV. SEM images in Figure 19b-d represent the morphology of coating when there is no power supply (0 kV) and when it is at 10 kV and 20 kV, respectively. Three distinct phenomena were observed. When there is no voltage, the solution is sprayed toward one focus circular section, as seen in Figure 19b. This condition obtains average WCA of 145.6º with remarkable standard deviation. After 5 measurements on different location of the coated surface, the maximum WCA is 154.54º and the minimum WCA is 136.66º. The maximum WCA is obtained when measuring inside the circular area. The minimum WCA is measured in the outer shell where only small amount of solution is reached. As the voltage increases to 10 kV (Figure 19c), the coating starts spreading more on the surface instead of focusing on one area, which results in higher WCA of 158.5º. However, the distribution of the coating is still uneven. The coating at 20kV condition is denser (Figure 19d). Figure 11e, f show magnified SEM images of the coated layer at 20 kV. From the thickness and distribution comparison, it is clear that

higher voltage results in a higher WCA measurement. If neglecting the safety factor, higher WCA than 167.8° could be hypothetically achieved when continuing to experiment on higher voltage than 20 kV. The higher working voltage represents higher electrostatic force for the charged droplets. The results indicate the electrostatic force is critical on the coating distribution and quality, serving as a critical driving force to impact droplets' displacement on the substrates.

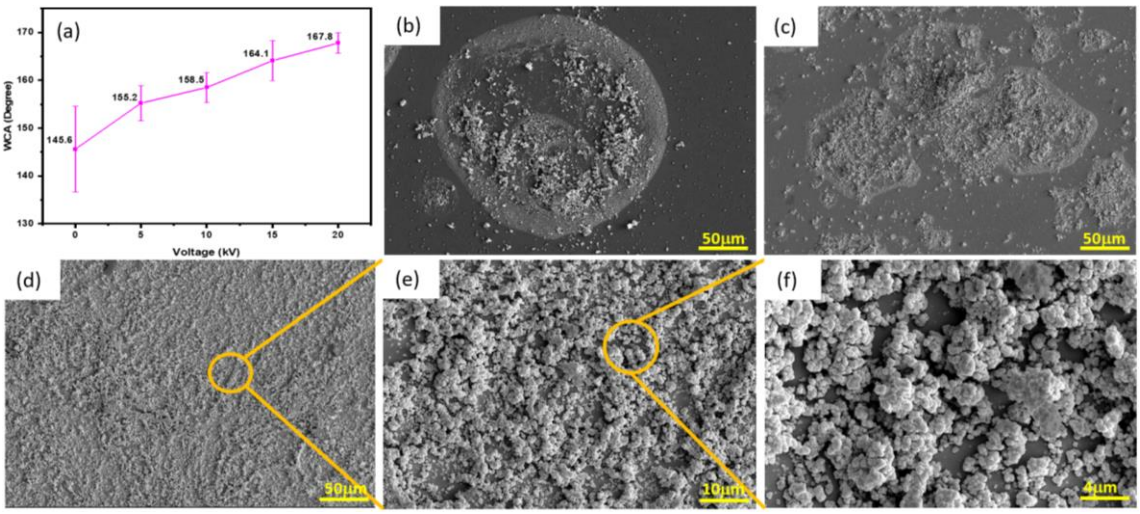


**Figure 19.** Effect of sprayed voltage. (a) WCA and sprayed voltage relation. SEM images of the coated surfaces at the sprayed voltage of (b) 0 kV, (c) 10 kV, and (d,e,f) 20 kV.

**6. Effect of sprayed time**

Various spraying periods were selected to study the effect of surface modification on the surface wetting behavior**.** Figure 20a shows the WCA values in relation to the sprayed periods. The graph does not show significant differences in CA values at different time. All the samples result in hydrophobic surfaces, in which their WCA is greater than 150°. Figure 20b-d represent the surface morphology of the coating at 15 mins, 1 hour, and 2 hours spraying, respectively. SEM images show that all samples have similar structure of small piles of particles packed on top of each other with voids in between. These structures create the adequate roughness for the surface to trap air and reduce the solid-liquid contact area. The superhydrophobic behavior can be achieved in the short period of spray time, as evidenced by the fact that 15 mins result in similar WCA measurement as 2.5 hours. Therefore, it is unnecessary to run the electrospraying process for a long time since there is not much difference in surface morphology between the spray times. It is concluded that once enough coverage is achieved, the extended spray time will not make significant impact on surface structure and WCA. According to this set of experiments,

one-hour experiment results in highest WCA value of 169.4°. The one-hour spraying period was determined to spray the coating that combines all the optimal factors in this study.

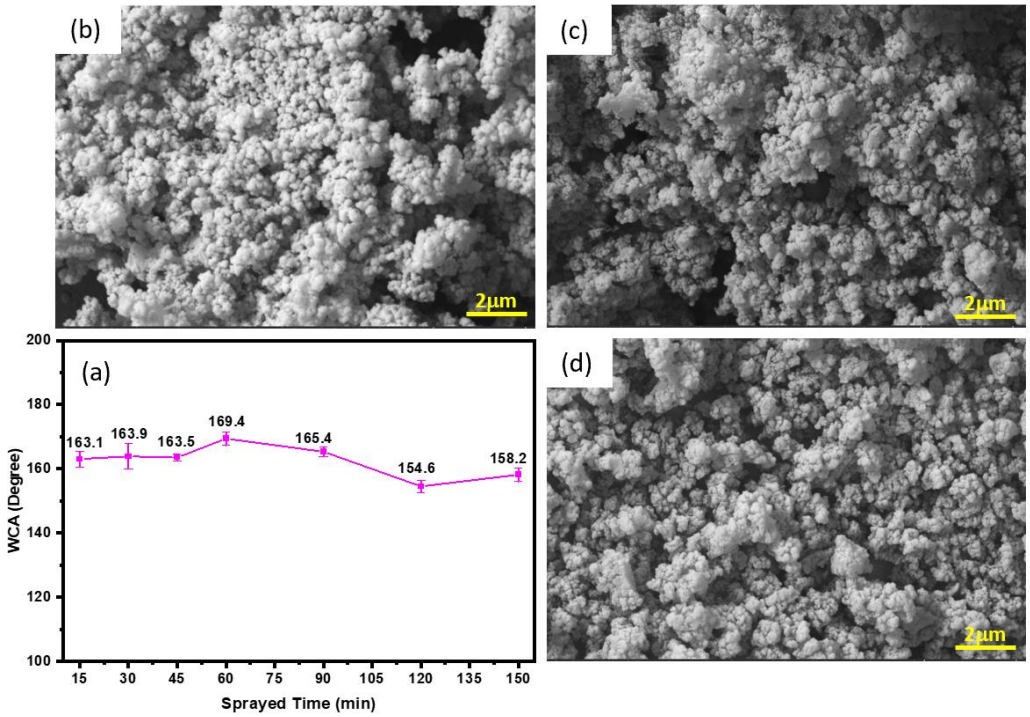


**Figure 20.** Effect of sprayed time. (a) Relationship between WCA and sprayed time on superhydrophobic performances. SEM images of the coated surfaces at the sprayed time of (b) 15 mins, (c) 1 hour, and (d) 2 hours.

### 7. Effect of air flowrate

To better understand the effect of air flow of electrospray deposition on the superhydrophobic coating, the WCAs were determined at the various air flowrates, consisting of 2, 3, 4, 5, 6 L/min. The relationship between WCA and air flow is shown in Figure 21a. The coating maintains its superhydrophobic property when the air flowrate is less than 4 L/min. The higher air flow results in random solution direction deposited on the glass substrate, thus it leads to lower WCA with larger standard deviation of the coating distribution. The most superhydrophobic and uniform layer is achieved at the air flowrate of 3 L/min. At this air flowrate, the coating obtains dense roughness structure, as shown in SEM image of Figure 21c. Compared to the coating at air flowrate of 3 L/min, the air flowrate of 2 L/min results in similar roughness but less uniform structure (Figure 21b). The SEM image of the coating at the air flowrate of 5 L/min (Figure 21d) show significant reduction in roughness structure as well as uniformity. Because the force of air

flow now dominates the particle movement and direction rather the electrostatic forces. It also indicates the balance of electrostatic force and air force is very crucial. Therefore, the selected air flowrate for the air-assisted electrospray deposition is 3 L/min.

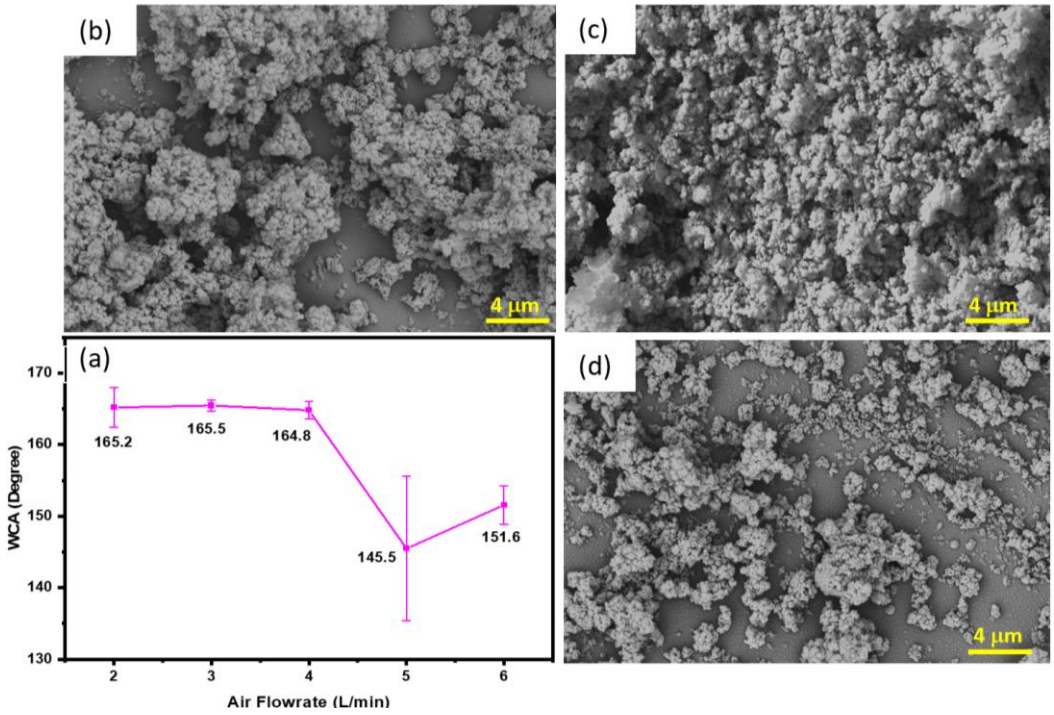


**Figure 21.** Effect of air flowrate. (a) Relationship between WCA and sprayed time on superhydrophobic performances. SEM images of the coated surfaces at the air flowrate of (b) 2 L/min, (c) 3 L/min, and (d) 5 L/min.

**8. Coating with optimal factors combination and other properties**

To verify whether the parameters always have a positive interaction effect, the superhydrophobic coating was prepared by using the combination of the optimal solution concentrations and air-assisted electrospray parameters identified above. As discussed in previous sections, these parameters are chosen to be 50mg PAN and 200mg $SiO_2$ in DMF solution, 20 kV power supply, 30 µL/min solution infused rate, and 3 L/min of air flowrate. The prepared coating obtains the static contact angle of 167.1° which is superhydrophobic, whereas the pristine borosilicate glass contact angle is 46.8° which is completely wetted. It is also noted the obtained contact angel with the selected parameters is close to but not the highest number in this study, indicating that not all factors interfere in a positive way. In addition, the coated surface before CVD of trichloro (1H, 1H, 2H, 2H-perfluorooctyl) silane is completely wetted during water drop test, whereas it exhibit superhydrophobic property after CVD. Superhydrophobic surface can

be successfully achieved only if two main criteria are met, which are roughness structure and low surface energy. $SiO_2$/PAN solution was fabricated on a glass surface through air-assisted electrospray method and then was cured at high temperature to create roughness structure. Since $SiO_2$ is hydrophilic, the roughness structure remains hydrophilic which results in a completely wetted surface. Trichloro (1H, 1H, 2H, 2H-perfluorooctyl) silane is a low-surface-energy material, therefore, the coated surface after CVD obtains both roughness structure and low surface energy, which results in a superhydrophobic surface. Without $SiO_2$ rough structure, the trichloro (1H, 1H, 2H, 2H-perfluorooctyl) silane coated glass has contact angle of 105.53°. The coating thickness was found to be 28.2 μm (Figure 22b). The transparency and superhydrophobicity are mutually exclusive, which means higher roughness structure leads to light scattering, thus it reduces the transparency.[3] In this study, the transmittance percentage is determined to evaluate the transparency of the surface. The transmittance spectra of the superhydrophobic surface and a pristine glass is demonstrated in Figure 22a. For the wavelength above 500nm, the transmittance of superhydrophobic surface in this study is above 60%, which is reduced by less than 30% as compared to that of pristine glass. Even with the reduction in transmittance compared to the pristine glass, this transparency of the prepared superhydrophobic surface is still well-reflected in the easy readability of letters underneath the coated glass substrate (Figure 22c). Thickness control and more ordered nanostructures will be explored as continuing effort to increase transparency, so that the application can be extended to electronics screen.

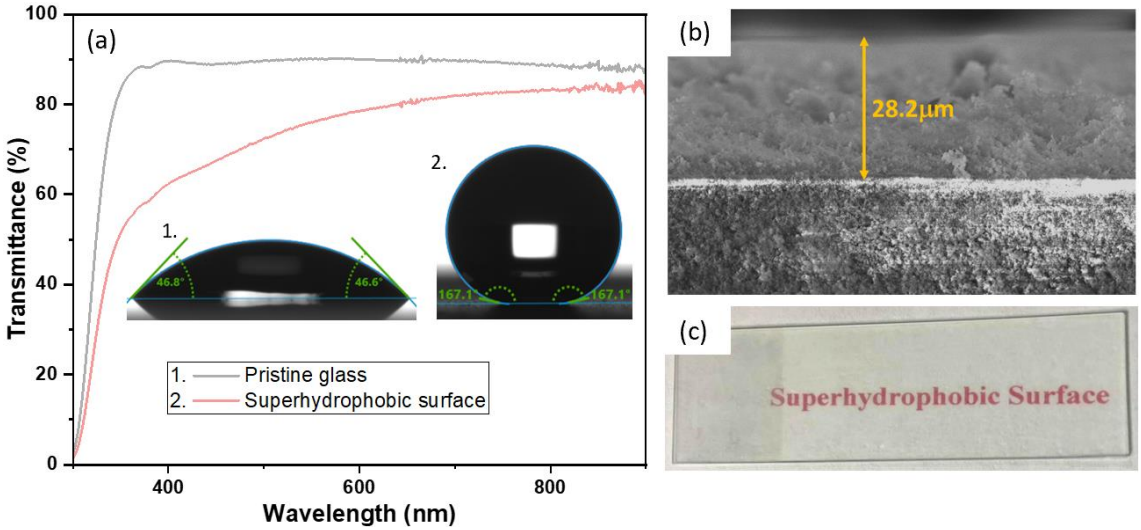


**Figure 22.** Properties of the superhydrophobic surface**.** (a) Ultraviolet-visible transmittance spectra of superhydrophobic surface compared to pristine glass. The insert images shows a water droplet with its static contact angle on a pristine glass and on

superhydrophobic surface. (b) Cross-sectional SEM image of coated glass substrate. (c) Photo showing transparency of the printed text behind the glass slide coved with superhydrophobic coating.

**9. Applications**

The prepared superhydrophobic surface shows remarkable performance on super repelling of the common water solutions, such as milk, coffee, tea, and orange juice. In addition, the low wetting behavior with extremely non-polar liquids, such as cooking oil and hexadecane is demonstrated in Figure 23. The droplets of all the liquids did not wet the surface and exhibit typical spherical shapes. The water solutions obtained static contact angles above 164$^{o}$ which well-perform super repellency. Cooking oil and hexadecane exhibit static contact angle above 141$^{o}$ which represents low wetting behavior. The coated superhydrophobic surface is nonpolar. Water is polar while cooking oil and hexadecane are non-polar. Therefore, non-polar cooking oil/ hexadecane molecules tend to have more interaction with the nonpolar superhydrophobic surface, which results in the inferior wetting behavior of the surface toward cooking oil and hexadecane compared to water based solution. The self-cleaning functionality of the coatings was experimented with 1 mg carbon black particles deposited on the coated surface. Multiple droplets were injected and rolled off of the surface which is placed at the angle of 20$^{o}$ from the flat table surface. As seen in Figure 23b-c, carbon black particles were significantly removed after depositing water droplets on the surface which well-highlighted its self-cleaning functionality. Figure 23d-e are time-resolved images of a 6μL water droplet depositing on small amount carbon black particles on a pristine glass and the superhydrophobic surface. As seen in Figure 23d, the surface is rapidly wetted after water dropping on the pristine glass surface, showing no self-cleaning capability. On the other hand, the water droplet remains attached to the needle after injecting to the superhydrophobic surface (Figure 23e) which demonstrates the significantly low surface tension of the coating. Therefore, the water droplet is able to be lifted up from the superhydrophobic surface with carbon black particles as the needle moved up. After two lifting cycles, there is no carbon black particle left on the surface which represents good self-cleaning functionality of the prepared coating.

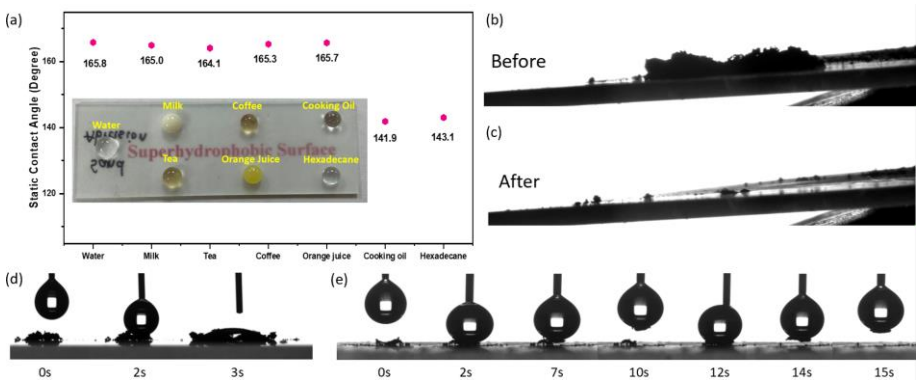


**Figure 23.** Application of the superhydrophobic surface. (a) Static contact angles of different liquids on the prepared superhydrophobic substrate. The insert image is photograph of different liquids on the coated surface. The images of carbon black particles on the coated surface (b) before and (c) after dropping multiple water droplets on the surface. These images were captured by contact angle measurement instrument. Time-resolved images of the carbon black picking up by 6µl water droplet on (d) uncoated glass substrate and (e) the superhydrophobic surface.

## 10. Reliability of the coated layer

Abrasion examination is one of the universal methods used for evaluating the durability of superhydrophobic surface against the physical force.[8, 67, 68] In this report, sandpaper abrasion was performed to demonstrate the reliability of the superhydrophobic coating to different harsh environmental conditions. The WCAs of the coated glass slide before and after abrasion cycles are shown in Figure 24a. The WCA of the as-prepared glass slide is 167.2°. The WCA decreases in the first three abrasion cycles and then it starts increasing and reaches 167.2° at the fifth cycle. Afterwards, the WCA slightly decreases as abrasion cycles increases. The thick coating layer of 28.2µm (Figure 22b) results in lower adhesion of the top particle namely, more loose structure. Thus, the top loose particles of the coating were first removed in the first three sandpaper abrasion cycles while maintaining the roughness structure. Five abrasion cycles exhibit thinner coated layer with better adhesive force to the glass substrate, thus it results in increasing WCA to 167.2°. Thus, the coated layer possesses better transparency, but its structure remains as rough as it is before abrasion. This result indicates the thinner coating with the same superhydrophobicity is possible. Even though the WCA slightly decrease after the fifth cycles, the coated glass slide retained its strong water repellent characteristics after 30 abrasion cycles, displaying good mechanical robustness. In addition, tape adhesion test was considered to study the mechanical robustness of the as-prepared superhydrophobic coating. Subsequently a 3M double-sided tape was harshly pressed onto the coated

surface, scratched, hold for 10 seconds, and torn off. The relations between WCA and peeling cycles were demonstrated in Figure 24b. The coating retains its superhydrophobicity during the tested peeling cycles.

The durability of the superhydrophobic coating against strong acid and base environments were also studied in this paper. The coated layer appeared to remain the same with no peeling after interacting with acid and base solution. The WCA measurements did not fluctuate significantly after acid and base examination which concludes that the superhydrophobic surface has excellent anti-acid and anti-base capability. Before acid/base testing, the two coated surfaces obtained 154.79° ± 1.30° and 153.45° ± 0.95°. After immersing in acid/base solution, WCA of the two coatings are 156.94° ± 1.21° and 152.9° ± 4.87° in acid and in base solution, respectively. An additional experiment to rinse off the coated surface with DI water after acid/base tests followed by drying in air at room temperature was studied. The coating remains with strong adhesion on glass substrate with no peeling off. The WCA measurements in this case were similar to the one without rinsing with DI water. Therefore, rinsing off with water did not affect the durability of the surface as well as superhydrophobic property.

The outdoor exposure examination was investigated to determine the durability of the coated superhydrophobic surface. The humidity within 15 days drastically varied between 39 and 93%. The temperature ranges from 37 to 72°F. The weather conditions are quite diverse, such as cloudy, windy, breezy, clear, calm, sunny, and light rainy. Water contact angle measurements of the coated surface for outdoor exposure experiment is presented in Figure 24c. The surface retained its superhydrophobic property throughout the diversity of weather conditions. The WCA of the coated glass slide were 161.35° and 155.05° before and after 15 days exposing the outdoor environment. As a result, the mechanical robustness of the coating withstands well a variety of weather climates.

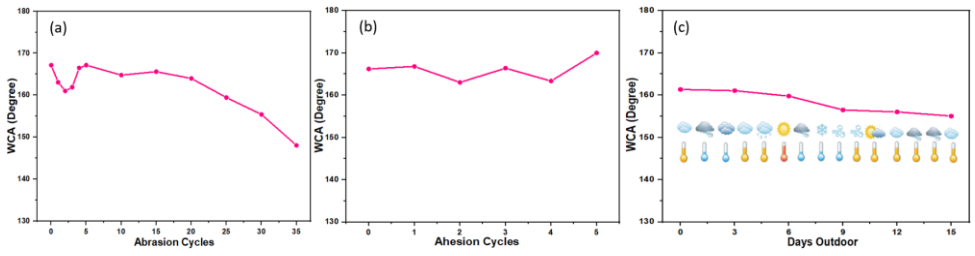


**Figure 24.** Reliability of the coated layer. WCAs measured after (a) sandpaper abrasion (b) adhesion cycles (c) outdoor exposure examination on the as-prepared surface.

# Conclusions and Recommendations

In conclusion, this report presented a facile air-assisted electrospray technique to prepare a self-cleaning superhydrophobic surface. The influence of coating precursor compositions and spraying conditions on the surface properties were thoroughly analyzed. The coated surface exhibited a remarkable water and oil repellent characteristic and good mechanical robustness toward harsh abrasion conditions. Furthermore, the coatings show an excellent self-cleaning performance. Thus, this simple and straightforward method represents an import technique addition to the current field of self-cleaning coating for various potential engineering and daily use applications. It is also found the optical transmittance of the coating was lower than 85% throughout a broad spectrum of ultraviolet and visible wavelengths. Improving transparency of the coating via different precursor solutions and thinner coatings are the two planned directions in our continuing research for electronics screen applications.

# Acronyms, Abbreviations, and Symbols

| Term | Description |
|---|---|
| AA- | Air-assisted- |
| $Al_2O_3$ | Aluminum oxide |
| CA | Contact angle |
| $CF_2$ | Difluoromethylene group |
| $CF_3$ | Trifluoromethyl group |
| $CH_2$ | Methylene group |
| $CH_3$ | Methyl group |
| CVD | Chemical vapor deposition |
| DI | Deionized |
| DMF | N,N-Dimethylformamide |
| FESEM | Field emission scanning electron microscope |
| HCl | Hydrochloric acid |
| ITO | Indium titanium oxide |
| LTRC | Louisiana Transportation Research Center |
| LV | Liquid vapor |
| NaOH | Sodium hydroxide |
| NASA | National Aeronautics and Space Administration |
| NSF | National Sanitation Foundation |
| PAN | Polyacrylonitrile |
| PANI | Polyaniline |
| PET | Polyethylene terephthalate |
| PTFE | Polytetrafluoroethylene (Teflon) |
| PTES | Perfluorodecyltriethoxysilane |
| PTMS | Trimethoxypropylsilane |
| SA | Sliding angle |
| SAN | Styrene-acrylonitrile |
| SCA | Static contact angle |
| SEM | Scanning electron microscope |
| $SiO_2$ | Silicon dioxide |
| SL | Solid liquid |
| SV | Solid vapor |
| TEM | Transmission electron microscope |

| Term | Description |
|---|---|
| UV-vis | Ultraviolet-visible |
| WCA | Water contact angle |
| ZnO | Zinc oxide |

# References


[1] Li, W.; Amirfazli, A. Microtextured Superhydrophobic Surfaces: A Thermodynamic Analysis. Adv. Colloid Interface Sci. 2007, 132 (2), 51−68.

[2] Milne, A. J. B.; Amirfazli, A. The Cassie Equation: How It Is Meant to Be Used. Adv. Colloid Interface Sci. 2012, 170 (1−2), 48− 55.

[3] Fei, L.; He, Z.; LaCoste, J. D.; Nguyen, T. H.; Sun, Y. A Mini Review on Superhydrophobic and Transparent Surfaces. Chem. Rec. 2020, 20 (11), 1257−1268.

[4] Li, Y.; Zhang, R.; Yu, H.; Chen, G.; Zhu, M.; Qiu, B.; Zou, H.; Li, X. Fluorinated Nanosilica Size Effect on Hierarchical Structure and Superhydrophobic Properties of the Epoxy Nanocomposite Film. ACS Appl. Polym. Mater. 2020, 2 (2), 418−426.

[5] Butt, H. J.; Roisman, I. V.; Brinkmann, M.; Papadopoulos, P.; Vollmer, D.; Semprebon, C. Characterization of Super LiquidRepellent Surfaces. Curr. Opin. Colloid Interface Sci. 2014, 19 (4), 343−354.

[6] Xue, C. H.; Guo, X. J.; Ma, J. Z.; Jia, S. T. Fabrication of Robust and Antifouling Superhydrophobic Surfaces via Surface-Initiated Atom Transfer Radical Polymerization. ACS Appl. Mater. Interfaces 2015, 7 (15), 8251−8259.

[7] Xue, Z.; Wang, S.; Lin, L.; Chen, L.; Liu, M.; Feng, L.; Jiang, L. A Novel Superhydrophilic and Underwater Superoleophobic HydrogelCoated Mesh for Oil/Water Separation. Adv. Mater. 2011, 23 (37), 4270−4273.

[8] Huang, J.; Yang, M.; Zhang, H.; Zhu, J. Solvent-Free Fabrication of Robust Superhydrophobic Powder Coatings. ACS Appl. Mater. Interfaces 2021, 13 (1), 1323−1332.

[9] Jeon, Y.; Nagappan, S.; Li, X. H.; Lee, J. H.; Shi, L.; Yuan, S.; Lee, W. K.; Ha, C. S. Highly Transparent, Robust Hydrophobic, and Amphiphilic Organic-Inorganic Hybrid Coatings for Antifogging and Antibacterial Applications. ACS Appl. Mater. Interfaces 2021, 13 (5), 6615−6630.

[10] Nundy, S.; Ghosh, A.; Mallick, T. K. Hydrophilic and Superhydrophilic Self-Cleaning Coatings by Morphologically Varying ZnO Microstructures for Photovoltaic and Glazing Applications. ACS Omega 2020, 5 (2), 1033−1039.

[11] Bayer, I. S. On the Durability and Wear Resistance of Transparent Superhydrophobic Coatings. Coatings 2017, 7 (1), 12.

[12] Doganci, M. D. Fabrication of Superhydrophobic Transparent Cyclic Olefin Copolymer (COC)-SiO2 Nanocomposite Surfaces. J. Appl. Polym. Sci. 2021, 138 (14), 50145.

[13] Manifar, T.; Rezaee, A.; Sheikhzadeh, M.; Mittler, S. Formation of Uniform Self-Assembly Monolayers by Choosing the Right Solvent: OTS on Silicon Wafer, a Case Study. Appl. Surf. Sci. 2008, 254 (15), 4611−4619.

[14] Siddiqui, A. R.; Li, W.; Wang, F.; Ou, J.; Amirfazli, A. One-Step Fabrication of Transparent Superhydrophobic Surface. Appl. Surf. Sci. 2021, 542, 148534.

[15] Janowicz, N. J.; Li, H.; Heale, F. L.; Parkin, I. P.; Papakonstantinou, I.; Tiwari, M. K.; Carmalt, C. J. Fluorine-Free Transparent Superhydrophobic Nanocomposite Coatings from Mesoporous Silica. Langmuir 2020, 36 (45), 13426−13438.

[16] Zhao, S.; Zhao, J.; Wen, M.; Yao, M.; Wang, F.; Huang, F.; Zhang, Q.; Cheng, Y. B.; Zhong, J. Sequentially Reinforced Additive Coating for Transparent and Durable Superhydrophobic Glass. Langmuir 2018, 34 (38), 11316−11324.

[17] Zheng, H.; Pan, M.; Wen, J.; Yuan, J.; Zhu, L.; Yu, H. Robust, Transparent, and Superhydrophobic Coating Fabricated with Waterborne Polyurethane and Inorganic Nanoparticle Composites. Ind. Eng. Chem. Res. 2019, 58 (19), 8050−8060.

[18] Teshima, K.; Sugimura, H.; Inoue, Y.; Takai, O.; Takano, A. Transparent Ultra Water-Repellent Poly(Ethylene Terephthalate) Substrates Fabricated by Oxygen Plasma Treatment and Subsequent Hydrophobic Coating. Appl. Surf. Sci. 2005, 244 (1−4), 619−622.

[19] Hao, L.; Gao, T.; Xu, W.; Wang, X.; Yang, S.; Liu, X. Preparation of Crosslinked Polysiloxane/SiO 2 Nanocomposite via in Situ Condensation and Its Surface Modification on Cotton Fabrics. Appl. Surf. Sci. 2016, 371, 281−288.

[20] Zhu, X.; Zhang, Z.; Ren, G.; Men, X.; Ge, B.; Zhou, X. Designing Transparent Superamphiphobic Coatings Directed by Carbon Nanotubes. J. Colloid Interface Sci. 2014, 421, 141−145.

[21] Kim, M.; Kim, K.; Lee, N. Y.; Shin, K.; Kim, Y. S. A Simple Fabrication Route to a Highly Transparent Super-Hydrophobic Surface with a Poly(Dimethylsiloxane) Coated Flexible Mold. Chem. Commun. 2007, 22, 2237−2239.

[22] Cavalli, A.; Mugele, F. Superamphiphobic Surfaces. In Droplet Wetting and Evaporation; Brutin, D., Ed.; Elsevier Inc.: 2015; p 57..

[23] Chen, C.; Weng, D.; Chen, S.; Mahmood, A.; Wang, J. Development of Durable, Fluorine-Free, and Transparent Superhydrophobic Surfaces for Oil/Water Separation. ACS Omega 2019, 4 (4), 6947−6954.

[24] Fei, L.; Yoo, S. H.; Villamayor, R. A. R.; Williams, B. P.; Gong, S. Y.; Park, S.; Shin, K.; Joo, Y. L. Graphene Oxide Involved AirControlled Electrospray for Uniform, Fast, Instantly Dry, and BinderFree Electrode Fabrication. ACS Appl. Mater. Interfaces 2017, 9 (11), 9738−9746.

[25] Lee, J. H.; Kang, J.; Kim, S. W.; Halim, W.; Frey, M. W.; Joo, Y. L. Effective Suppression of the Polysulfide Shuttle Effect in LithiumSulfur Batteries by Implementing RGO-PEDOT:PSS-Coated Separators via Air-Controlled Electrospray. ACS Omega 2018, 3 (12), 16465−16471.

[26] Heo, K. J.; Oh, H. J.; Eom, H.; Kim, Y.; Jung, J. H. HighPerformance Bag Filter with a Super-Hydrophobic Microporous Polytetrafluoroethylene Layer Fabricated by Air-Assisted Electrospraying. Sci. Total Environ. 2021, 783, 147043.

[27] Niknejad, A. S.; Bazgir, S.; Kargari, A.; Barani, M.; Ranjbari, E.; Rasouli, M. A High-Flux Polystyrene-Reinforced Styrene-Acrylonitrile/Polyacrylonitrile Nanofibrous Membrane for Desalination Using Direct Contact Membrane Distillation. J. Membr. Sci. 2021, 638, 119744.

[28] Lee, J.; Ko, B.; Kang, J.; Chung, Y.; Kim, Y.; Halim, W.; Lee, J. H.; Joo, Y. L. Facile and Scalable Fabrication of Highly Loaded Sulfur Cathodes and Lithium−Sulfur Pouch Cells via Air-Controlled Electrospray. Mater. Today Energy 2017, 6, 255−263

[29] a) B. Bhushan, Y. C. Jung, Prog. Mater. Sci. 2011, 56, 1–108; b) S. Parvate, P. Dixit, S. Chattopadhyay, J. Phys. Chem. B 2020, 124, 1323–1360; c) M. Ma, R. M. Hill, Curr. Opin. Colloid Interface Sci. 2006, 11, 193–202.

[30] a) C. H. Xue, X. J. Guo, J. Z. Ma, S.-T. Jia, ACS Appl. Mater. Interfaces 2015, 7, 8251–8259; b) W. Hou, Y. Shen, J. Tao, Y. Xu, J. Jiang, H. Chen, Z. Jia, Colloids Surf. A 2020, 586, 124180; c) C. Qi, H. Chen, L. Shen, X. Li, Q. Fu, Y. Zhang, Y. Sun, Y. Liu, ACS Appl. Mater. Interfaces 2020, 3, 2047– 2057; d) T. Xiang, Y. Han, Z. Guo, R. Wang, S. Zheng, S. Li, C. Li, X. Dai, ACS Sustainable Chem. Eng. 2018, 6, 5598– 5606; e) Y. C. Liu, W. J. Huang, S. H. Wu, M. Lee, J. M. Yeh, H. H. Chen, Corros. Sci. 2018, 138, 1–7; f) W. Jiang, J. He, F. Xiao, S. Yuan, H. Lu, B. Liang, Ind. Eng. Chem. 2015, 54, 6874–6883; g) Z. Sun, T. Liao, K. Liu, L. Jiang, J. H. Kim, S. X. Dou, Small 2014, 10, 3001–3006; h) D. Wang, Q. Sun, M. J. Hokkanen, C. Zhang,

F. Y. Lin, Q. Liu, S. P. Zhu, T. Zhou, Q. Chang, B. He, Q. Zhou, L. Chen, Z. Wang, R. H. A. Ras, X. Deng, Nature 2020, 582, 55–59.

[31] a) G. Barati Darband, M. Aliofkhazraei, S. Khorsand, S. Sokhanvar, A. Kaboli, Arab. J. Chem. 2020, 13, 1763–1802; b) S. Das, S. Kumar, S. K. Samal, S. Mohanty, S. K. Nayak, Ind. Eng. Chem. 2018, 57, 2727–2745; c) P. Zhang, F. Y. Lv, Energy 2015, 82, 1068–1087.

[32] a) S. Yu, Z. Guo, W. Liu, Chem. Commun. 2015, 51, 1775– 1794; b) Y. Zhang, B. Dong, S. Wang, L. Zhao, L. Wan, E. Wang, RSC Adv. 2017, 7, 47357–47365; c) P. Wang, M. Chen, H. Han, X. Fan, Q. Liu, J. Wang, J. Mater. Chem. A 2016, 4, 7869–7874.

[33] T. Aytug, US Department of Energy (DOE) report, ORNL/ TM-2015/197.

[34] T. Huhtamäki, X. Tian, J. T. Korhonen, R. H. A. Ras, Nat. Protoc. 2018, 13, 1521–1538.

[35] Y. X. Song, PhD thesis, University of Nebraska – Lincoln, 2018.

[36] a) J. Zimmermann, S. Seeger, F. A. Reifler, Text. Res. J. 2009, 79, 1565–1570; b) J. T. Korhonen, T. Huhtamaki, O. Ikkala, R. H. Ras, Langmuir 2013, 29, 3858–3863.

[37] H. J. Ensikat, P. Ditsche-Kuru, C. Neinhuis, W. Barthlott, Beilstein J. Nanotechnol. 2011, 2, 152–161.

[38] A. Tuteja, W. Choi, G. H. McKinley, R. E. Cohen, M. F. Rubner, MRS Bull. 2008, 33, 752–758.

[39] L. Gao, T. McCarthy, Langmuir 2006, 22, 2966–2967.

[40] T. Young, Philos. Trans. R. Soc. London Ser. B 1805, 95, 65–87.

[41] R. N. Wenzel, Ind. Eng. Chem. 1936, 28, 988–994.

[42] A. B. D. Cassie, S. Baxter, Trans. Faraday Soc. 1944, 40, 546– 551.

[43] a) R. J. Vrancken, H. Kusumaatmaja, K. Hermans, A. M. Prenen, O. Pierre-Louis, C. W. M. Bastiaansen, D. J. Broer, Langmuir 2010, 26, 3335–3341; b) M. Lundgren, N. L. Allan, T. Cosgrove, Langmuir 2007, 23, 1187–1194; c) H. Y. Erbil, C. E. Cansoy, Langmuir 2009, 25, 14135–14145.

[44] Dupont, Ti-pure titanium dioxide titanium dioxide for coatings, 2007.

[45] E. Brinkman, Blog to be found under http://www.betase.nl/ advancedceramics/light-transmission-of-aluminium-oxide/? lang=en, 2017.

[46] Y. Li, E. Vasileva, I. Sychugov, S. Popov, L. Berglund, Adv. Opt. Mater. 2018, 6, 1800059.

[47] Y. Chen, Y. Zhang, L. Shi, J. Li, Y. Xin, T. Yang, Z. Guo, Appl. Phys. Lett. 2012, 101, 033701

[48] K. L. Cho, I. I. Liaw, A. H. F. Wu, R. N. Lamb, J. Phys. Chem. C 2010, 114, 11228–11233.

[49] a) R. G. Karunakaran, C. H. Lu, Z. Zhang, S. Yang, Langmuir 2011, 27, 4594–4602; b) J. Li, Z. Huang, F. Wang, X. Yan, Y. Wei, Appl. Phys. Lett. 2015, 107, 051603.

[50] S. Zhao, J. Zhao, M. Wen, M. Yao, F. Wang, F. Huang, Q. Zhang, Y. B. Cheng, J. Zhong, Langmuir 2018, 34, 11316– 11324.

[51] S. Y. Lee, Y. Rahmawan, S. Yang, ACS Appl. Mater. Interfaces 2015, 7, 24197–24203.

[52] a) S. G. Lee, D. S. Ham, D. Y. Lee, H. Bong, K. Cho, Langmuir 2013, 29, 15051–15057; b) Y. Li, X. Men, X. Zhu, B. Ge, F. Chu, Z. Zhang, J. Mater. Sci. 2016, 51, 2411–2419; c) Z. Liang, M. Geng, B. Dong, L. Zhao, S. Wang, Surf. Eng. 2019, 1–8.

[53] L. Xu, R. Karunakaran, J. Guo, S. Yang, ACS Appl. Mater. Interfaces 2012, 4, 1118–1125.

[54] R. A. Alawajji, G. K. Kannarpady, A. S. Biris, Appl. Surf. Sci. 2018, 444, 208–215.

[55] D. Ebert, B. Bhushan, Langmuir 2012, 28, 11391–11399.

[56] I. Bayer, Coating 2017, 7.

[57] G. Wang, H. Wang, Z. Guo, Chem. Commun. (Camb.) 2013, 49, 7310–7312.

[58] Y. Gao, I. Gereige, A. El Labban, D. Cha, T. T. Isimjan, P. M. Beaujuge, ACS Appl. Mater. Interfaces 2014, 6, 2219–2223.

[59] K. Yadav, B. R. Mehta, J. P. Singh, Appl. Surf. Sci. 2015, 346, 361–365.

[60] T. Aytug, A. R. Lupini, G. E. Jellison, P. C. Joshi, I. H. Ivanov, T. Liu, P. Wang, R. Menon, R. M. Trejo, E. Lara-Curzio, S. R. Hunter, J. T. Simpson, M. P. Paranthaman, D. K. Christen, J. Mater. Chem. C 2015, 3, 5440–5449.

[61] X. Deng, L. Mammen, H. J. Butt, D. Vollmer, Science 2012, 335, 67.

[62] J. E. Mates, R. Ibrahim, A. Vera, S. Guggenheim, J. Qin, D. Calewarts, D. E. Waldroup, C. M. Megaridis, Green Chem. 2016, 18, 2185–2192.

[63] C. Chen, D. Weng, S. Chen, A. Mahmood, J. Wang, ACS Omega 2019, 4, 6947–6954.

[64] T. Verho, C. Bower, P. Andrew, S. Franssila, O. Ikkala, R. H. A. Ras, Adv. Mater. 2011, 23, 673–678.

[65] a) L. Xu, Z. Geng, J. He, G. Zhou, ACS Appl. Mater. Interfaces 2014, 6, 9029–9035; b) N. Yokoi, K. Manabe, M. Tenjimbayashi, S. Shiratori, ACS Appl. Mater. Interfaces 2015, 7, 4809– 4816.

[66] Halim, W.; Lee, J. H.; Park, S. M.; Zhang, R.; Sarkar, S.; O'Neil, T.; Chiang, Y. C.; Joo, Y. L. Directly Deposited Binder-Free Sulfur Electrode Enabled by Air-Controlled Electrospray Process. ACS Appl. Energy Mater. 2019, 2 (1), 678−686.

[67] She, Z.; Li, Q.; Wang, Z.; Li, L.; Chen, F.; Zhou, J. Researching the Fabrication of Anticorrosion Superhydrophobic Surface on Magnesium Alloy and Its Mechanical Stability and Durability. Chem. Eng. J. 2013, 228, 415−424.

[68] Liu, M.; Li, J.; Hou, Y.; Guo, Z. Inorganic Adhesives for Robust Superwetting Surfaces. ACS Nano 2017, 11 (1), 1113−1119.